JCI The Journal of Clinical Investigation

GIGYF1 disruption associates with autism and impaired IGF-1R signaling

Guodong Chen, Bin Yu, Senwei Tan, Jieqiong Tan, Xiangbin Jia, Qiumeng Zhang, Xiaolei Zhang, Qian Jiang, Yue Hua, Yaoling Han, Shengjie Luo, Kendra Hoekzema, Raphael A. Bernier, Rachel K. Earl, Evangeline C. Kurtz-Nelson, Michaela J. Idleburg, Suneeta Madan Khetarpal, Rebecca Clark, Jessica Sebastian, Alberto Fernandez-Jaen, Sara Alvarez, Staci D. King, Luiza L.P. Ramos, Mara Lucia S.F. Santos, Donna M. Martin, Dan Brooks, Joseph D. Symonds, Ioana Cutcutache, Qian Pan, Zhengmao Hu, Ling Yuan, Evan E. Eichler, Kun Xia, Hui Guo

J Clin Invest. 2022. https://doi.org/10.1172/JCI159806.

Research In-Press Preview Genetics Neuroscience

Graphical abstract

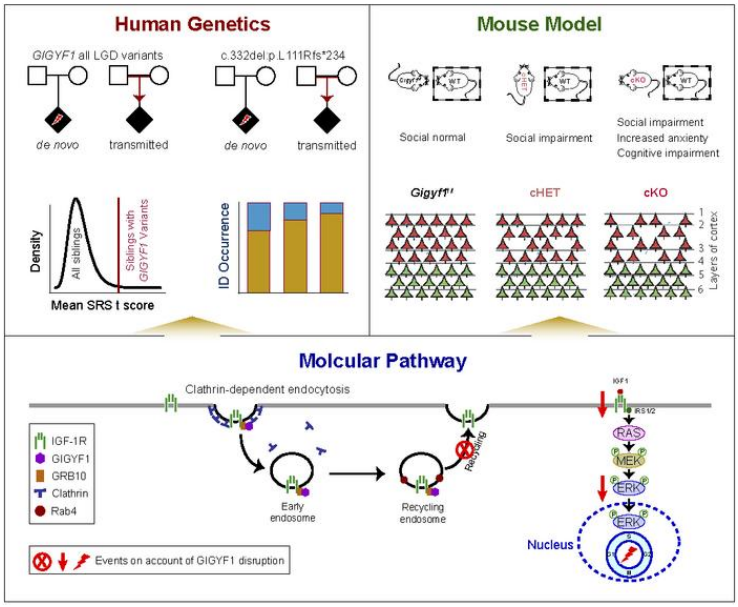

Find the latest version:

https://jci.me/159806/pdf

GIGYF1 disruption associates with autism and impaired IGF-1R signaling

Guodong Chen[1,19], Bin Yu[1,19], Senwei Tan[1,19], Jieqiong Tan[1,19], Xiangbin Jia[1], Qiumeng Zhang[1], Xiaolei Zhang[1], Qian Jiang[1], Yue Hua[1], Yaoling Han[1], Shengjie Luo[1], Kendra Hoekzema[2], Raphael A. Bernier[3], Rachel K. Earl[3], Evangeline C. Kurtz-Nelson[3], Michaela J. Idleburg[4], Suneeta Madan-Khetarpal[4], Rebecca Clark[4], Jessica Sebastian[5], Alberto Fernandez-Jaen[6], Sara Alvarez[7], Staci D. King[8], Luiza L.P. Ramos[9,10], Mara Lucia S.F. Santos[11], Donna M. Martin[12], Dan Brooks[12], Joseph D. Symonds[13], Ioana Cutcutache[14], Qian Pan[1], Zhengmao Hu[1], Ling Yuan[1], Evan E. Eichler[2,15], Kun Xia[1,16,17], Hui Guo[1,18*]

[1]Center for Medical Genetics and Hunan Key Laboratory of Medical Genetics, School of Life Sciences, Central South University, Changsha, Hunan 410078, China; [2]Department of Genome Sciences, University of Washington School of Medicine, Seattle, WA 98195, USA; [3]Department of Psychiatry, University of Washington, Seattle, WA 98195, USA; [4]Department of Medical Genetics, UPMC Children's Hospital of Pittsburgh, Pittsburgh, PA, USA; [5]Department of Human Genetics, University of Pittsburgh, Pittsburgh, PA, USA; [6]Department of Pediatric Neurology, Hospital Universitario Quirónsalud, Madrid, Spain; School of Medicine, Universidad Europea de Madrid, Spain; [7]Department of Genomics and Medicine, Genomics and Medicine, NIMGenetics, 28108 Madrid, Spain; [8]Department of Neurology, Baylor College of Medicine, Houston, TX, US; [9]Mendelics Genomic Analysis, Sao Paulo 04013, Brazil; [10]Neurogenetics Unit, Department of Neurology, University of Sao Paulo, Sao Paulo, 01308-000, Brazil. [11]Neuropediatric Division, Hospital Pequeno Principe, Curitiba, Paraná, Brazil; [12]Department of Pediatrics, Michigan Medicine, University of Michigan, Ann Arbor, MI, USA; [13]Paediatric Neurosciences Research Group, Royal Hospital for Children, Glasgow, UK; [14]Translational Medicine, UCB Pharma, Slough, UK; [15]Howard Hughes Medical Institute, University of Washington, Seattle, WA 98195, USA; [16]CAS Center for

Excellence in Brain Science and Intelligences Technology (CEBSIT), Chinese Academy of Sciences, Shanghai 200000, China; [17]Hengyang Medical School, University of South China; [18]Hunan Key Laboratory of Animal Models for Human Diseases, Changsha, Hunan 410078, China. [19]These authors share first authorship: Guodong Chen, Bin Yu, Senwei Tan, Jieqiong Tan.

Address correspondence to: Hui Guo, Center for Medical Genetics and Hunan Key Laboratory of Medical Genetics, School of Life Sciences, Central South University, Changsha, Hunan 410078, China. Phone: 086-0731-84805340; Email: guohui2@csu.edu.cn.

Abstract

Autism spectrum disorder (ASD) represents a group of neurodevelopmental phenotypes with a strong genetic component. Excess of likely gene-disruptive (LGD) mutations of *GIGYF1* was implicated in ASD. Here, we reported that *GIGYF1* was the second most mutated gene among known ASD high-confidence risk genes. We investigated the inheritance of 46 *GIGYF1* LGD variants, including the highly recurrent mutation, c.333del:p.L111Rfs*234. Inherited *GIGYF1* heterozygous LGD variants were 1.8 times more common than *de novo* mutations. Unlike most high-confidence genes, ASD individuals with *GIGYF1* LGD variants were less likely to have cognitive impairments. Using a *Gigyf1* conditional knockout mouse model, we showed that haploinsufficiency in the developing brain led to social impairments without significant cognitive impairments. In contrast, homozygous mice showed more severe social disability as well as cognitive impairments. *Gigyf1* deficiency in mice led to a reduction of upper layer cortical neurons accompanied by decreased proliferation and increased differentiation of neural progenitor cells. We showed that GIGYF1 regulated the recycling of IGF-1R to cell surface. Knockout of GIGYF1 led to a decreased level of IGF-1R on the cell surface disrupting the IGF-1R/ERK signaling pathway. In summary, our findings showed that GIGYF1 was a regulator of IGF-1R recycling. Haploinsufficiency of *GIGYF1* was associated with autistic behaviors likely through interference with IGR-1R/ERK signaling pathway.

Introduction

Autism spectrum disorder (ASD) is a highly heritable neurodevelopmental condition characterized by impaired social communication and repetitive behaviors (1). Previous studies have identified over 200 high-confidence ASD risk genes—most of which are based on significant enrichments of *de novo* variants in ASD families (https://gene.sfari.org/). Besides ASD, the majority of high-confidence genes are also enriched for *de novo* variants in other neurodevelopment disorders (NDDs) associated with intellectual disability (ID) and developmental delay (DD) (2, 3). Because of the extreme rarity of the pathogenic variants within these high-penetrance genes, the exact mutation and inheritance patterns and detailed phenotypic associations of most ASD risk genes are still largely unknown.

GIGYF1 encodes a protein involved in the insulin-like growth factor (IGF) receptor signaling pathway (4). The first evidence for its role in ASD risk was the identification of three *de novo* likely gene-disruptive (LGD) variants in three unrelated ASD individuals by screening over 2,500 families from the Simons Simplex Collection (SSC) cohort (5, 6). A recently study using a larger sample size confirms a genome-wide significant enrichment of *GIGYF1 de novo* LGD variants in ASD individuals (7). In addition, an excess of *de novo* LGD variants in *GIGYF1* was also recently reported in DD (3). Despite these findings, its inheritance among ASD families and phenotypic association of this specific gene are still not well-characterized. More importantly, how *GIGYF1* is involved in the mechanisms underpinning neurodevelopment and autistic behaviors is completely unknown.

In this study, we combine human genetics, conditional knockout models and molecular studies to highlight the role of *GIGYF1* in the neurobiology of ASD. We report both an excess of *de novo* LGD mutations and transmission disequilibrium of inherited *GIGYF1* LGD mutations among ASD

individuals with low cognitive impairment occurrence and discover ASD endophenotypes among carriers without ASD diagnosis. We show that haploinsufficiency of *Gigyf1* in mouse leads to social and behavioral disabilities without significant cognitive impairments. Mechanistically, disruption of GIGYF1, a new regulator of IGF-1R recycling, leads to inactivation of the IGF-1R/ERK signaling pathway which likely affects neurodevelopment and autistic behaviors by disrupting the neural progenitor cell (NPC) cycle dynamics early in brain development.

Result

Mutation pattern and inheritance mode of *GIGYF1* heterogenous LGD variants

To comprehensively delineate the mutation pattern and inheritance modes of *GIGYF1* variants in ASD, we analyzed whole-exome sequencing (WES) or whole-genome sequencing (WGS) data from two autism cohorts: the Simons Foundation Powering Autism Research (SPARK) (8) and Simons Simplex Collection (SSC) (9) (Methods). Combined, the collection includes 20,452 families with one or both biological parents available (23,351 ASD cases) and 12,227 ASD cases without parental data (Supplemental Table 1). We identify 35 high-confidence *GIGYF1* LGD variants in 60 ASD individuals from 55 families or singleton cases (Figure 1A and Supplemental Figure 1; Supplemental Table 2). Six of them are *de novo*, 15 are transmitted, and one is *de novo* or transmitted in different families. The inheritance of the other 13 variants is unknown due to lack of parental data. In addition, we also identify eight non-transmitted *GIGYF1* LGD variants in parents without ASD diagnoses and three LGD variant transmitted or *de novo* to siblings (without ASD diagnoses) only (Figure 1A and Supplemental Figure 1; Supplement Table 2). We found that transmission of LGD mutations is 1.8 times more likely than *de novo* mutations among ASD families where both biological parents are available to study. We found a significant *de novo* enrichment ($P < 2.7 \times 10^{-12}$) and significant transmission disequilibrium ($P < 1 \times 10^{-5}$) of *GIGYF1*

heterozygous LGD variants in the two cohorts. Importantly, we found that the frequency of *GIGYF1* LGD variants ranks second among known ASD high-confidence genes (Figure 1B).

Interestingly, a recurrent LGD variant (c.332del:p.L111Rfs*234) is detected in 23 ASD individuals from 20 families or singleton cases (Figure 1, A and B). This variant occurred *de novo* in four ASD individuals and was transmitted in nine ASD individuals (Figure 1C). In addition, this variant is also observed in two siblings without ASD diagnoses (one inherited and one *de novo*) and one unaffected parent who did not transmit this variant to offspring (Figure 1C). *De novo* occurrence of this variant in ASD is significantly higher than random occurrence in the general population even using a gene-level mutation rate as background (P = 0.0004). Significant transmission disequilibrium was also observed for this specific variant (P = 0.03). To characterize the functional effect of this variant, we constructed the wild-type (WT) and mutant plasmids and performed immunoblotting and immunostaining in HEK293T cells and HeLa cells. We reveal that the p.L111Rfs*234 variant produced a truncated protein with remarkable increased expression and abnormal localization (Supplemental Figure 2 and Supplemental Figure 3). The WT protein localizes predominantly to cytoplasm; in contrast to the mutant, which is restricted to the nuclei. The abnormal localization was also observed in Neuro2a cells (Supplemental Figure 3) and mouse primary cultured neurons (Figure 1D).

In addition to the variants detected in the SPARK and SSC cohorts, we recruited an additional seven new cases with *GIGYF1* heterozygous LGD variants (three *de novo*, one inherited and three of unknown inheritance) (Figure 1A) and one case with *de novo* missense variant through a network of international collaborators connected by GeneMatcher (10), as well as collecting the detailed phenotype information (Supplemental Table 3, Supplementary Table 4). Five of the six individuals with ASD assessments were diagnosed as ASD. Of note, the recurrent variant

p.L111Rfs*234 was transmitted in a family with substantial autism history (Supplemental Figure 4).

Phenotypic association of *GIGYF1* heterozygous LGD variants

To delineate *GIGYF1*-associated ASD and NDD phenotypes, we first analyzed the severity of the core symptoms of ASD individuals with *GIGYF1* LGD variants. We computed the scores on two scales, the Social Communication Questionnaire (SCQ) and the Repetitive Behaviors Scale–Revised (RBS-R) (Supplemental Table 5) which represent the severity of social communication and repetitive behaviors respectively. We found that the mean of SCQ ($P = 0.75$) and RBS-R ($P = 0.30$) scores (Methods) of ASD individuals with *GIGYF1* LGD variants were comparable to all ASD individuals in SPARK cohort, indicating *GIGYF1* monoallelic LGD variants lead to average severity level of social impairments and repetitive behaviors (Figure 2A).

Known ASD high-confidence genes associate with substantial cognitive impairments (11). To explore the cognition association with *GIGYF1* heterozygous LGD variants, we compared the occurrence of the parent-reported cognitive impairment in SPARK. ASD individuals with *GIGYF1* LGD variants are less likely to have cognitive impairments compared to known high-confidence ASD genes (SFARI gene score = 1) (28% vs. 12%, $P = 8.5 \times 10^{-24}$). Although not significant, the frequency of cognitive impairment in ASD individuals with *GIGYF1* LGD variants is lower (12% vs. 19%, $P = 0.28$) than all ASD individuals in SPARK (Figure 2B and Supplemental Table 5). ASD individuals with the recurrent site have similar frequency of cognitive impairments with all ASD individuals with *GIGYF1* LGD variants (15% vs. 12%). These data indicate *GIGYF1* heterozygous LGD variants may associate with better cognitive outcome. To explore the co-occurring conditions pattern of *GIGYF1* LGD variants, we compared the rate of the parent-reported behavior problems, DD, and neuropsychiatric problems in SPARK clinical dataset

(Methods) (Supplemental Table 6). We found that the rate of parent-reported behavior problems (40.9% vs 39.8%, $P = 0.88$), DD (70.5% vs 63.4%, $P = 0.43$), and neuropsychiatry problems (38.6% vs 37.8%, $P = 1$) in ASD individuals with *GIGYF1* LGD variants are all comparable to ASD individuals without *GIGYF1* LGD variants in the SPARK cohort (Figure 2C and Supplemental Table 7).

There are eight siblings without ASD diagnoses (five in SPARK and three in SSC) that carry *GIGYF1* LGD variants. We found that two of the five siblings in SPARK have parent-reported language and/or motor developmental delay, which shows a marginally significant higher rate (40% vs 8%, $P = 0.053$) relative to parent reports of language and motor developmental delay in siblings without ASD and *GIGYF1* LGD variants (Figure 2D), although the sample size is too small to get a conclusion. For the three SSC siblings, we reveal that unaffected siblings with *GIGYF1* LGD variants have poorer social ability, as reflected by the Social Responsiveness Scale (SRS) score in the SSC, compared to siblings without ASD and *GIGYF1* LGD variants ($P = 0.004$, Figure 2E and Supplemental Table 8). In addition to siblings with *GIGYF1* LGD variants but without ASD diagnoses, we also found 23 parents without ASD diagnosis but with transmitted or non-transmitted *GIGYF1* LGD variants. We compared the co-occurring conditions in these parents (21/23 with clinical data available), and parents without ASD diagnosis and without *GIGYF1* LGD variants (Figure 2F). We found that the frequency of behavior problems (23.8% vs. 9.6%), DD (9.5% vs. 4.3%), and neuropsychiatry problems (47.6% vs. 38%) are all higher (1.3-2.5 times) in parents with *GIGYF1* LGD variants, however, only the behavior problems show statistical significance ($P = 0.045$) (Supplemental Table 7) under the current small sample size. These data indicate that *GIGYF1* heterozygous LGD variants might also associate with ASD/NDD

endophenotypes in children without ASD diagnosis. Larger sample sizes are needed to further confirm this association.

Gigyf1 haploinsufficiency in nervous system leads to social and behavior impairments in mice

To explore the functions of *GIGYF1* in developing brain and autistic behavior in vivo, we knocked out exons 1-9 of *Gigyf1* and generated floxed (*Gigyf1*$^{f/f}$) mice with conditional alleles carrying loxP sites in introns 1 and 9 by CRISPR/Cas9 targeting strategy (Supplemental Figure 5A). The *Gigyf1*$^{f/f}$ mice were crossed with Nestin-Cre mice to generate *Gigyf1*$^{f/w}$-Cre^{Nestin} (cHET) and *Gigyf1*$^{f/f}$-Cre^{Nestin} (cKO) mice (Supplemental Figure 5B). Both *Gigyf1* cHET and cKO mice were viable. Immunoblot analysis showed that the cHET mice is haploinsufficiency for Gigyf1 and the cKO mice loses Gigyf1 expression (Supplemental Figure 5C). We found that the body weight of cKO was significantly decreased at postnatal day 30 (P30). No difference was observed in the cHET mice (Supplemental Figure 6).

We first performed a three-chamber social test for voluntary initiation of social interaction and discrimination of social novelty (12). In social interaction tests, *Gigyf1*$^{f/f}$ (we used as control in the mouse analysis) and cHET mice spent more time with social targets (Figure 3A, Stranger1) compared to an inanimate object (Figure 3A). However, the social interaction preference index of cHET was significantly lower than *Gigyf1*$^{f/f}$ mice. There was no difference in time spent between social targets and inanimate objects by cKO (Figure 3A). In social novelty tests, as expected, *Gigyf1*$^{f/f}$ mice spent more time with new social targets (Stranger2) compared to the similar mouse (Stranger1) (Figure 3A). Yet, there was no difference in time spent between Stranger2 and Stranger1 in both cHET and cKO mice (Figure 3A). These data suggest that both haploinsufficiency and homozygous knockout of *Gigyf1* in the developing brain impair social communication. We then performed a range of tests to evaluate the potential repetitive and

stereotyped behaviors (Figure 3, B and C). In marble burying tests, both cHET and cKO bury more marbles compare to *Gigyf1*$^{f/f}$ (Figure 3B). We also observed that cHET and cKO preferred to rearing (Figure 3C). We found no difference in the grooming and digging tests (Figure 3C). Considering that the marble burying test is more likely to reflect the anxiety behavior comparing with repetitive behavior and there is no significant difference in the grooming test, these data suggest that haploinsufficiency and homozygous knockout of *Gigyf1* in the developing brain has mild effect on repetitive behaviors in mice.

To determine whether *Gigyf1* deficiency leads to anxiety-like behaviors in mice, we introduced the Elevated plus maze (EPM) test, Open field (OF) test and Light-dark box (LDB) test. In EPM tests (Figure 3D), the cHET mice displayed similar time and distance in the open arm compared to *Gigyf1*$^{f/f}$ mice; however, the cKO mice showed significantly reduced time and travel distance in the open arm compared to *Gigyf1*$^{f/f}$ mice. In OF tests (Figure 3E), we also found the cKO mice tend to stay in the corner and rarely pass through the middle area compared to the *Gigyf1*$^{f/f}$ mice. There is no significant difference between cHET and *Gigyf1*$^{f/f}$ mice. Consistently, in LDB tests (Figure 3F), the cKO mice showed an significant increase in the preference to the dark box compared to *Gigyf1*$^{f/f}$ mice. This increase is not significant in cHET mice. These results indicate that *Gigyf1* haploinsufficiency in the developing brain has a very mild effect on the anxiety-like behavior in mice. This is in contrast to homozygous knockout *Gigyf1*, which showed remarkable anxiety-like behaviors.

To test learning and memory problems in *Gigyf1* knockout mice, we subjected the mice to the Morris water maze (MWM) test to evaluate the cognition of *Gigyf1* cHET and cKO mice. In MWM tests (Figure 3G), *Gigyf1* cKO mice showed a decreased latency to discover targets during training trials, as well as a decreased latency to reach the target region during the probe trial compared to

the *Gigyf1*$^{f/f}$ mice. However, this difference was not observed in cHET mice. Considering that the lower weight in the cKO mice might affect the performance on the MWM test, we subjected the mice to the novel-object recognition (NOR) test. In NOR tests (Figure 3H), *Gigyf1* cKO mice also showed a decrease in the total time exploring and in the discrimination index to the non-familiar object. These results suggest that *Gigyf1* haploinsufficiency has no significant impact on learning and memory in mice. Homozygous knockout *Gigyf1* in mice leads to severe learning and memory problems.

Gigyf1 deficiency leads to a reduction of the upper cortical layers in mouse

Growing evidence indicates that disrupted neocortical neurogenesis contributes substantially ASD pathogenesis (13, 14). Using the transcriptome data from BrainSpan, we revealed that *GIGYF1* is expressed broadly in human prenatal and postnatal brain with a slightly higher in the prenatal stage (Supplemental Figure 7A). By western blot, we revealed a similar pattern of Gigyf1 expression in mice cortex. Gigyf1 is highly expression in mouse prenatal cortex compared to postnatal cortex, especially at E14.5 and E18.5 (Supplemental Figure 7B). To investigate the role of *Gigyf1* in embryonic cortical development, we first evaluated the overall brain size and cortical cytoarchitecture. We found that the *Gigyf1* cKO mice at P2 showed a mild decrease in cortical area and cortical length when compared to than *Gigyf1*$^{f/f}$ mice (Figure 4A). No significant changes are observed in cHET mice. To explore whether *Gigyf1* deficiency changes the number of neurons in different cortical layers, we performed immunohistochemistry of layer-specific markers in the neocortex at E18.5. We detect fewer upper layer neurons labeled with markers Satb2 and Brn2 in both cHET and cKO compared to *Gigyf1*$^{f/f}$ cortex (Figure 4, B and C). We did not observe a significant difference in the numbers of deeper layer neurons including Tbr1^{+} and Ctip2^{+} cells in

cHET and cKO cortex (Figure 4D). These data indicate that *Gigyf1* deficiency leads to reduction of the upper cortical neurons.

Gigyf1 deficiency leads to decreased NPC proliferation

The abnormalities of the cerebral cortex are thought to be due to the proliferation, differentiation, or migration of NPCs (15, 16). To explore the role of *Gigyf1* in NPC development, we first examined the numbers of $Pax6^+$ radial glial cells (RGCs) and $Tbr2^+$ intermediate progenitor cells (IPCs) in the cHET and cKO cortex at E14.5. We observe that both $Pax6^+$ RGCs and $Tbr2^+$ IPCs are decreased (Figure 4E) indicating that *Gigyf1* deficiency decreases the NPC pool.

To confirm that *Gigyf1* is indispensable for NPC proliferation and/or migration, we performed pulse-labeling experiments with Edu at E14.5 and analyzed brains at either 30 min or 4 days after pulse-labeling with Edu. We found that the migration of cHET and cKO remain unchanged at E18.5 (Supplemental Figure 8). We observed that Edu^+ cells was decreased in both cHET and cKO cortex at E14.5 (Figure 4F). However, the $Pax6^+Edu^+/Pax6^+$ cells was increased in cKO cortex (Figure 4F) indicating that *Gigyf1* deficiency may lead to NPCs stay in the S phase and decrease the NPCs proliferation. To further determine whether the decreased NPCs proliferation is responsible for the decreased NPC pool, we performed immunohistochemistry of Ph3. We observed that $Ph3^+$ cells and $Ph3^+Pax6^+$ cells are both decreased in cHET and cKO cortex (Figure 4F), which is in consistent with the reduction of NPCs. To further validate that *Gigyf1* deficiency leads to prolonged S phase of NPCs, we labeled S phase NPCs by giving pregnant dams sequential Brdu and Edu pulses separated by a 1.5h interval at E14.5; we then analyzed Brdu and Edu single- and double-labeled NPCs by immunohistochemistry to deduce the duration of S phase (T_S) (Figure 4G, Methods). We found that the Ts of cHET and cKO NPCs are significantly longer when

compared to the *Gigyf1*$^{f/f}$ NPCs (Figure 4G). Similarly, increases of Ts are also observed in cHET and cKO embryos at E12.5 (Supplemental Figure 9).

To explore whether Gigyf1 has a functional role in NPCs differentiation, we performed pulse-labeling experiments with Edu at E14.5 and analyzed brains after 24h. We found that the differentiation of NPCs in cHET and cKO cortex was accelerated compared with *Gigyf1*$^{f/f}$ cortex (Figure 4H). Taken together, these results suggest that loss of *Gigyf1* in early brain development leads to a reduction of upper layer neurons, possibly linked to perturbations of proliferation and differentiation dynamics during cortical neurogenesis.

GIGYF1 deletion interferes with IGF-1R/ERK signaling pathway

The above data indicate that GIGYF1 plays a critical role in NPC proliferation and neurogenesis and that its mutation dysregulates the cell cycles during NPC development. Therefore, we further explore the potential underlying molecular mechanisms of how GIGYF1 regulates the NPC development. Previous studies have shown that the GYF domain of GIGYF1 binds to Grb10, an adapter protein which, in turn, binds to IGF-1R (17). A GIGYF1 fragment containing the GYF domain interacts with IGF-1R at 2 min after IGF-1 stimulation (4). To further characterize the interaction of full-length GIGYF1 with IGF-1R, we performed a series of co-immunoprecipitation experiments. We found that Flag-tagged IGF-1R interacted with HA-tagged GIGYF1 (Figure 5A). Meanwhile, purifying HA-tagged GIGYF1 interacted with Flag-tagged IGF-1R. To further validate the interaction between GIGYF1 and IGF-1R, we performed double immunofluorescence experiments and found that GIGYF1 co-localizes with IGF-1R and GRB10 (Figure 5B and Supplemental Figure 10). These results are consistent with the previous implication that GIGYF1 forms a complex with IGF-1R and GRB10 (4).

IGF-1R is a plasma transmembrane receptor that is activated by IGF-1, which, in turn, activates the downstream ERK and AKT-mTOR pathway (18). Previous knockdown and overexpression studies support both negative and positive regulatory effect of GIGYF1 or its GYF domain on IGF-1R signaling, thus leaving its physiological role on IGF-1R signaling unclear (4, 19). To further clarify the function of GIGYF1 on IGF-1R signaling, we constructed GIGYF1 KO cell lines using HEK293T cells to determine whether *GIGYF1* deficiency is involved in IGF-1R induced signaling. We stimulated cells with IGF-1 at 0, 2, 5, 7, 10, and 30 min, and then assessed for phosphorylation of IGF-1R (pIGF-1R), pERK, and pAKT. We found that pIGF-1R/IGF-1R at 10 and 30 min of IGF-1 stimulation are significantly decreased in *GIGYF1* KO cells compared to control cells (Figure 5C). Consistently, pERK/ERK at 7 and 10 min of IGF-1 stimulation is also decreased. Although we observed slight decrease of pAKT at 0, 2, and 5 min of IGF-1 stimulation, this difference is not significant. To determine that whether haploinsufficiency of *GIGYF1* also interferes this pathway, we stimulated cells with IGF-1 at 0, 5 and 7 min in *GIGYF1* heterozygous cells, and then assessed for phosphorylation of pERK. We found that pERK/ERK at 7 min of IGF-1 stimulation is also significantly decreased (Supplemental Figure 11). These results support that the *GIGYF1* haploinsufficiency and deletion decreases pIGF-1R/pERK signaling pathway.

To further elucidate whether GIGYF1 was involved in the regulation of the ERK pathway, we performed a rescue experiment by expressing WT plasmids of GIGYF1 in GIGYF1 KO cells under IGF-1 stimulation for 0, 2, 5, 7, 10, and 30 min (Figure 5D). WT plasmids of GIGYF1 significantly increased the pERK level after 5 and 7 min of IGF-1 stimulation. To explore whether disorder-related variants interfere with the ERK pathway, we performed a second rescue experiment using the recurrent *GIGYF1* LGD variant (p.L111Rfs*234) and another two LGD variants identified from our in-house cases (p.G174Efs*171 and p.E885*—one from the N-terminal and one from

the C-terminal, Supplemental Figure 2) after 7 min of IGF-1 stimulation. We found that all three *GIGYF1* LGD variants failed to rescue the decreased pERK level (Figure 5E). These data further validate that *GIGYF1* knockout and disorder-related LGD variants perturb the IGF-1R/ERK signaling pathway.

GIGYF1 regulates IGF-1R recycling

The above data show GIGYF1 deficiency suppresses IGF-1R/ERK signaling pathway. However, how GIGYF1 regulates IGF-1R activation is completely unknown. The above data show that GIGYF1 mainly localizes to the cytoplasm in the form of vesicles (Figure 1D and 5B) reminiscent of endosome. It is also known that cell surface IGF-1R traffics through endosomal vesicles (20). Once internalized, IGF-1R is first trafficked to early endosomes and subsequently transported to late endosomes for degradation or recycling endosome for recycling back to the plasma membrane (21) (Supplemental Figure 12). Based on this, we hypothesized that GIGYF1 might mediate the internalization and trafficking of IGF-1R. To test our hypothesis, we conducted double immunofluorescence experiments using antibodies to specific endosome markers. Intriguingly, we observed that HA-tagged GIGYF1 strongly co-localizes with the recycling endosomal marker, Rab4 (Supplemental Figure 13). We also observed that HA-tagged GIGYF1 partially co-localizes with the coated vesicles marker, clathrin, and early endosomal markers, EEA1 and Rab5A (Supplemental Figure 13). However, HA-tagged GIGYF1 does not co-localize with lysosomes (Lamp1) and other endosomal markers, including Rab7 and Rab11 (Supplemental Figure 14). These results indicate that GIGYF1 might be involved in clathrin-mediated endocytosis and Rab4-mediated recycling of internalized IGF-1R.

To further explore whether GIGYF1 regulates the recycling of IGF-1R, we conducted a surface biotinylation assay (Methods) to detect surface expression of IGF-1R in *GIGYF1* KO cells. IGF-

1R levels on the cell surface of *GIGYF1* knockout cells is significantly lower compared to control cells (Figure 5F), but the total IGF-1R levels are not changed. In addition, the expression of TMEM98, an IGF-1R unrelated cell surface protein, remains unchanged suggesting that GIGYF1 specifically affects IGF-1R. We next performed a surface biotinylation recycling assay (Supplemental Figure 15) to explore the effect of *GIGYF1* knockout on IGF-1R expression in cytoplasm (Methods). Interestingly, we found that knockout of *GIGYF1* significantly increases the expression of IGF-1R in the cytoplasm, but the expression of IGF-1R is almost never detected in control cells (Figure 5G, lane 4 vs. lane 7). Taken together, these data demonstrate that GIGYF1 regulates the recycling of IGF-1R to plasma membrane. Deficiency of *GIGYF1* leads to decreased expression of IGF-1R in plasma membrane (Figure 5H).

Disturbance of IGF-1R/ERK signaling in early brain development of *Gigyf1* deficiency mice

To validate whether GIGYF1 interferes with the IGF-1R/ERK signaling pathway in vivo, we performed immunoblotting experiments to detect pIgf-1r and pErk in *Gigyf1* knockout mice at E14.5. We observed that pIgf-1r and pErk levels are significantly diminished in the cortical lysates of both cHET and cKO mice compared to *Gigyf1*$^{f/f}$ mice (Figure 6A). Consistently, immunohistochemistry of pErk reveals decreased fluorescence intensity of pErk in the cortex of cHET and cKO mice (Supplemental Figure 16). ERK activation plays a fundamental role for G1/S transition (22). In cell cycle regulation, ERK activity regulates the induction of cyclin D1 and the down-regulation of p27 (23). Since we observe disturbed NPC cell cycle dynamics in *Gigyf1* deficient mice, we next examined whether p27 and cyclin D1 were also dysregulated. We found significantly increased expression of p27 and decreased expression of cyclin D1 (Figure 6A). These data together indicate that altered cell cycle dynamics of NPCs are most likely the resulted of disruption of the IGF-1R/ERK signaling pathway due to the lack of *Gigyf1* in mouse.

We then test whether IGF-1 could rescue *GIGYF1*-related pathogenesis. We adopted neurosphere formation assays at E14.5. We recorded and measured the size of neurospheres at 0 days, 3 days, 5 days, and 7 days of culturing in vitro. We found that the diameter of cHET neurospheres are significantly smaller compared with *Gigyf1*$^{f/f}$ at 3 days, and the diameter of cKO neurospheres are significantly smaller at all time points (Figure 6, B and C) indicating the impaired proliferation of NPCs in cHET and cKO neurospheres which is consistent with the above observation. In contrast, IGF-1 stimulation could increase the proliferation ability in both cHET and cKO neurospheres (Figure 6, B and C). Specificly, IGF-1 stimulation could rescue the decreased diameter of neurospheres in cHET at all time points, and the decreased diameter of neurospheres in cKO at 5 days. IGF-1 stimulation could partially rescue the decreased diameter of neurospheres in cKO at 3 days and 7 days. These data indicate that IGF-1 can ameliorate the proliferation impairments in *Gigyf1*-deficient mice.

DISCUSSION

In this study, we comprehensively characterized the mutation pattern and inheritance modes of *GIGYF1* mutations using large, recently sequenced ASD cohorts. Our data confirm *de novo* enrichment of *GIGYF1* LGD variants and highlight the important contribution of inherited LGD variants in potential ASD risk. Notably, we report a recurrent frameshift variant, manifesting loss-of-function effect on ERK signaling activity, which accounts for 40% ASD individuals with *GIGYF1* LGD variants and explains 0.064% ASD individuals in the general population, emphasizing the importance of investigating rare, inherited recurrent variants in ASD or NDD risk even under a samples size with limited statistical power for this class of variants. The molecular basis for this recurrent deletion is unknown but we noticed that it is located adjacent to a polyguanine stretch. In yeast experimental assays, such polyG tracts (albeit typically longer 13+)

have been shown to increase mutability both locally and distally possibly through error-prone translation synthesis and repair pathways (24).

Our phenotypic association analysis reveals that ASD individuals with *GIGYF1* heterozygous LGD variants share ASD core symptoms but with a lower prevalence of cognitive impairment. Although *GIGYF1* LGD variants are also identified among family members without ASD diagnoses, we find evidence of ASD/NDD endophenotypes, such as language/motor developmental delay as well as social impairment. These findings suggest that *GIGYF1* may represent an important ASD risk gene underlying core ASD phenotypes without significant cognitive impairments. Indeed, our data show that the haploinsufficiency of *Gigyf1* in the mouse developing brain does not contribute to learning and memory deficits associated with cognitive impairments. In contrast, homozygous knockouts of *Gigyf1* in the developing brain cause more severe ASD core symptoms, anxiety-like behaviors, and severe cognitive problems consistent with a dosage effect of loss-of-function *Gigyf1* mutations on phenotypic severity.

The functional roles of GIGYF1 in neurodevelopment have not been previously characterized. During the early stage of embryonic neurodevelopment, NPCs in the ventricular zone (VZ) and the subventricular zone (SVZ) generate the complex cytoarchitecture and the final adult cortex as a result of NPC proliferative or neurogenic divisions. The balance of this process determines normal cortex composition and function (15, 16). Using our nervous system conditional knockout mouse model, we found that the dosage of Gigyf1 is essential for neocortical neurogenesis, which is strongly implicated in ASD pathology (14). Our data revealed reduced neurons of the upper but not deeper layers in *Gigyf1* deficient mice. The explanation might be that the reduction of ERK signaling pathway led to premature neurogenesis of NPCs in early stage which compensates for the presumed reduced deeper layer neurons (25). We proposed that *Gigyf1* deficiency alteres the

homeostasis of NPCs proliferation and differentiation which in turn affects the development of the cerebral cortex.

Regulation of cell cycle by the IGF-1R/ERK pathway has been well-characterized (26). Although GIGYF1 has been shown to be involved in the regulation of IGF-1R signaling pathway, the results were still contradictory (4, 19). In this study, we confirmed that *GIGYF1* deficiency reduced the pIGF-1R and down-regulated the downstream ERK signaling pathway. In addition, the *GIGYF1* LGD variants identified from ASD individuals were unable to rescue the decreased pERK, further supporting the hypothesis that IGF-1R/ERK dysregulation underlies, in part, the pathology of *GIGYF1*-related ASD individuals. Importantly, in vivo analysis further supports the dysregulation of the Igf-1r/Erk signaling pathway in *Gigyf1* deficient mice. Besides this reduction in the pIgf-1r/pErk, two critical cell cycle regulators, p27 and cyclin D1, were also perturbed in *Gigyf1* deficiency mice. We propose that the abnormal outcomes on neurogenesis and NPC proliferation are likely due to the disruption of the Igf-1r/Erk signaling pathway by loss of *Gigyf1*, although our study did not provide a clear causal evidence for disrupted Igf-1r/Erk signaling in the cortical neurogenesis and behavioral phenotypes observed in the cHET and cKO mice. Whether this is the causal, or a causal, factor in the phenotypes remains to be determined.

We also investigated how GIGYF1 regulates the IGF-1R signaling pathway. It is known that once IGF-1R is internalized, it is recycled, degraded, or translocated to the intracellular membrane compartments of the Golgi apparatus or the nucleus (21). We report that GIGYF1 strongly co-localizes with the recycling endosomal marker Rab4. Rab4 and Rab11 had been both proposed to be involved in the ‘fast’ and ‘slow’ recycling pathways, respectively (27). We do not detect co-localization of GIGYF1 with Rab11, indicating that GIGYF1 predominantly mediates the fast recycling pathway. Our surface biotinylation assay further confirms that GIGYF1 regulates the

recycling of GIGYF1 to the cell surface. These results suggest GIGYF1 as a novel regulator of IGF-1R recycling, which might be an important target for elucidating the recycling mechanisms specific for IGF-1R.

In summary, our study demonstrates that haploinsufficiency of *GIGYF1* in human and mouse leads to core autistic behaviors with less significant cognitive impairments. We propose that disruption of *GIGYF1*, a new regulator of IGF-1R fast recycling, leads to inactivation of IGF-1R/ERK signaling pathway contributing to neurodevelopment and autistic behaviors in mice through perturbation of normal the cell cycle dynamics of NPCs early in brain development. The discovery of inherited and *de novo GIGYF1* pathogenic variants in ASD individuals will enhance genetic diagnosis and studies of transmission within families, which is critical for genetic counselling especially among multiplex families. The mouse model and molecular insights further highlight the importance of the IGF-1R/ERK pathway in the molecular pathogenesis of ASD.

METHODS

WES and WGS data. The WES or WGS data of seven sub-cohorts of from SPARK(8) were included in this study, including SPARK_pilot, SPARK_WES1, SPARK_WES2, SPARK_WES3, SPARK_WGS1, SPARK_WGS2, and SPARK_WGS3. After removing the duplicates in the seven sub-cohorts, 68,560 individuals, including 33,241 ASD individuals with WES/WGS data passing QC, were included in our study. The WGS data of 2,337 trio or simplex quad families from the SSC(9) were used in this study. This study was approved by the Institutional Review Board (IRB) of Central South University (IRB #2019-1-17). VCF files of SPARK_pilot, SPARK_WES1, SPARK_WES2, SPARK_WES3, SPARK_WGS1, SPARK_WGS2, and SPARK_WGS3 were downloaded from SFARI Base (https://base.sfari.org/). BCFtools (28), VCFtools (29) and GATK (30) (v4.1.8.1) were applied to left-align, normalize, extract and filter rare LGD events (allele

frequency < 0.1% in gnomAD v2.1.1 non-neuro subset exomes (31) in the VCF files. We applied genotype quality (GQ), read-depth (RD) and allele balance (AB) filters for QC and variants filtering. LGD variants within 0.25 < AB < 0.75, DP > 10 and GQ > 25 were retained. All *GIGYF1* LGD mutations were visualized using Integrative Genomics Viewer (32) in order to get rid of likely variant calling artifacts. ANNOVAR (33) was used to annotate the variants.

De novo enrichment and transmission disequilibrium analysis. Excess of *GIGYF1 de novo* LGD variants was analysed using two probabilistic models (denovolyzeR (34) and CH model (35)). Briefly, we derived the expected number of *de novo* LGD events in a given population based on the mutability of *GIGYF1* and the number of probands sequenced and then compared the observed number of *de novo* LGD variants against expectation using a Poisson framework (denovolyzeR) or binomial model (CH model). We applied RV-TDT (36) for transmission disequilibrium analysis of *GIGYF1* LGD variants in 49 families with at least one parent data available.

Clinical data and analysis. For the SPARK cohort, clinical data used in this study was pulled from SPARK_Collection_Version6. Social Communication Questionnaire (SCQ) total score, Repetitive Behavior Scale-Revised (RBS-R) total score, and cognitive impairment conditions data were extracted from core_descriptive_variables.csv file. The clinical records of developmental delay (global developmental delay, speech and language delay, learning disability, motor delay or developmental coordination disorder), behavior problems (attention deficit-hyperactivity disorder (ADHD) or attention deficit disorder (ADD), conduct disorder, Intermittent explosive disorder, oppositional defiant disorder), and neuropsychiatric problems (anxiety disorder, bipolar (Manic-depressive) disorder, depression or dysthymia, disruptive mood dysregulation disorder, hoarding, obsessive-compulsive disorder, deparation anxiety, social anxiety disorder/social phobia, seizure disorder or epilepsy, personality disorder, schizophrenia, other psychosis or schizoaffective

disorder, Tourette syndrome or Tic disorder) were extracted from basic_medical_screening.csv file. For the SSC cohort, phenotype information is available from SSC Version 15.3 Phenotype Dataset. SCQ total score and SRS t score were derived from srs_parent.csv and scq_life.csv, respectively. Comparisons between groups were performed using Mann–Whitney U test (qualitative data) or Fisher's exact test (quantitative data). Down-sampling analysis was performed by permutation test (random sampling 1,000,000 times).

Mice. The *Gigyf1* conditional knockout mice were generated in GemPharmatech, Co., Ltd. Mice were housed in a constant temperature and humidity environment with relatively stable conditions (generally 22-24°C, 70% humidity, 12 hours of light and 12 hours of darkness) and allowed to feed and drink freely. The genetic background of all mice used in this study is C56BL/6J. Age- and sex-matched littermate pairs were used in the experiments.

Behavioral tests. All behavioral tests were performed using age-matched male littermates. The age of mice used for the first behavioral test is around 4 weeks. The age range of mice used for behavioral tests are 4-8 weeks. Mice had at least 24 h of rest time between tests. All experimental data were analyzed using AVTAS ver 5.0 single tracking, Animal Video Tracking Analysis System (AniLab Software and Instruments, guoj). All tests were conducted in a blind manner. Detailed methods for specific behavioral tests (three-chamber test, marbles bury test, digging, rearing and grooming test, morris water-maze test, light-dark box test, elevated plus maze test. open field test, novel-object recognition test) can be found in the Supplemental Methods.

Immunohistology. Immunohistology was performed on 20μm frozen tissue sections. Brain slices use local tissue structure for spatial matching to ensure accurate spatial comparison. The prepared brain slices were baked at 60°C for 2h. Frozen sections were washed with DPBS for 10 min, for BrdU staining, sections were treated with 2 M HCl at 37 °C for 30 min and 0.1 M sodium borate

buffer, pH 8.5, for 10 min at room temperature. They were then blocked with 5% BSA in 0.1% PBST for 1 h at room temperature. Sections were incubated overnight at 4℃ with primary antibodies (rabbit Tbr1; rabbit 488; rabbit Cy3; rabbit Pax6; rabbit Tbr2; rat BrdU; rabbit Ctip2; mouse Ph3; mouse Brn2). After washing three times with DPBS, secondary antibodies were applied to sections for 1 h at room temperature. Sections were stained with DAPI for 1min, covering the slices with a cover glass. Fluorescence images were acquired by Zeiss LSM 880 confocal microscope and analyzed in ImageJ software.

Injection of S-phase tracer. BrdU/EdU double-labeling was carried out according to Houlihan, S. L., et al (37). Briefly, pregnant females were injected intraperitoneally with 5-Bromo-2′-Deoxyuridine (BrdU, Sigma) (50 mg/kg body weight) and 1.5 h later with the same dose of 5-Ethynyl-2'- deoxyuridine (EdU, Sigma) and killed after 0.5 h. For EdU single-labeling, pregnant mice were injected intraperitoneally with EdU (50 mg/kg body weight) at E14.5 and killed after 0.5 h, 24h or 4 days. The obtained mouse brain slices for Edu immunohistochemistry using Click-iT™ Edu kit (C10338,Thermo Scientific).

Plasmids. Full-length *GIGYF1*, purchased from Youbio Biological Technology Company, was cloned into pCAGGS-IRES-GFP vector using SgsI and XhoI restriction sites. LGD mutations of *GIGYF1* (p.L111Rfs*234, p.G174Efs*171, p.E885*) were generated by site-directed mutagenesis using Phanta Max Super-Fidelity DNA Polymerase (P505-d1,Vazyme). Plasmids of pcDNA3.1-3xFlag-IGF-1R were purchased from Youbio Biological Technology Company.All constructs were confirmed by Sanger sequencing.

Cell culture and transfection. HEK293T cells (CBP60439, Cobioer) and HeLa cells (CBP60232, Cobioer) were cultured in DMEM medium with 10% fetal bovine serum (10100147, Thermo Scientific), 1% penicillin and streptomycin (15140122, Thermo Scientific,). All cells were cultured

at 37℃ in a humidified incubator with 5% CO2, Lipofectamine 3000 reagent (L3000015, Thermo Scientific,) were used to transfect following the manufacturer's protocol.

LentiCRISPR V2-mediated GIGYF1 knockout cells. SgRNA of GIGYF1 was designed through http://crispr.dfci.harvard.edu/SSC and synthesized DNA oligos were inserted into LentiCRISPR V2 vectors (52961, Addgene plasmid) by using FastDigest BsmBI (FD0454, Thermo Scientific). The constructs were confirmed by Sanger sequencing. HEK293T cells were transiently transfected with sgRNA, pCMV-VSV-G (8454, Addgene plasmid) and psPAX2 (12260, Addgene plasmid) for 2 days, then concentrated and pacificated were performed through ultrafiltration to obtain ultra-pure Lentivirus products. Lentiviruses infected HEK293T cells for 2 days followed by the addition of 2 μg/mL puromycin for 3 days. Cells were diluted to 96-well plates for monoclonal cell selection and successful knockouts were verified by western blot using antibody GIGYF1 from Bethyl.

Antibodies. The following primary antibodies were used: rabbit HA-tag (1:1000, CST, 3724s), rabbit Flag-tag (1:1000, CST, 14793s), rabbit Clathrin Heavy Chain (1:50, CST, 4796s), rabbit Caveolin-1 (1:200, CST, 3267s); rabbit EEA1 (1:200, CST, 3288s), mouse Rab5A (1:400, CST, 46449s), rabbit Rab4 (1:200, CST, 2167s), rabbit Rab11 (1:50, CST, 5589s), rabbit Rab7 (1:50, CST, 9367s), rabbit Lamp1 (1:100, CST, 9091s), rabbit phospho-IGF-1R-β (Tyr1131)/Insulin Receptor β (Tyr1146) (1:1000, CST, 3021s), rabbit IGF-1R-β (1:1000, CST, 9750s), rabbit phospho-Akt (Ser473) (1:1000, CST, 4060s), rabbit Akt (1:1000, CST, 9272s), phospho-p44/42 MAPK (Thr202/Tyr204)(1:1000, CST, 4370s), rabbit p44/42 MAPK (1:1000, CST, 9102s), rabbit p27 Kip1 (1:1000, CST, 3686s), rabbit Cyclin D1 (1:1000, CST, 55506s), rabbit Tbr1 (1:400, CST, 49661s), rabbit Ki67 (1:400, CST, 9129s), rabbit Grb10 (1:1000, Santa Cruz, sc-74509), mouse IGF-1R-α (1:1000, Santa Cruz, sc-81464), mouse Brn2 (1:100, Santa Cruz, sc-393324), rabbit Satb2 (1:500, Abcam, ab92446), rabbit Tbr2 (1:100, Abcam, ab23345), rat BrdU (1:500, Abcam,

ab6326), rabbit Ctip2 (1:100, Abcam, ab18465), rabbit 488 (1:500, Thermo Scientific, SA5-10018) and rabbit Cy3 (1:500, Thermo Scientific, A10522), chicken GFP (1:500, Aves Labs, GFP-1020), rabbit Pax6 (1:100, BioLegend, PRB-278P), rabbit GIGYF1 (1:1000, Bethyl, A304-132A-M), mouse Ph3 (1:2000, Millipore-Sigma, 07-424) and rabbit TMEM98 (1:1000, Millipore-Sigma, HPA053385).

Immunofluorescence assay. HeLa cells were grown in 12-well plates about 30-50% confluence and were transiently transfected with 1.5 µg of expression plasmid. After 24 h, cells were washed with PBS and fixed with 4% paraformaldehyde (V900894-100G, Sigma-Aldrich) for 10 min, and then blocked with 5% BSA (FA016-25G, Genview) in 0.1% PBST for 1 h at room temperature. Cells were incubated overnight at 4℃ with primary antibodies. After washing three times with PBS, cells were incubated with corresponding secondary antibodies for 1 h at room temperature. Cells were stained with DAPI (D9542, Sigma-Aldrich) for 1 min. Covering the cells with a cover glass and then fluorescence was visualised by confocal microscopy (341-H, Leica).

Western blot assay. *GIGYF1* KO HEK293T cells and control HEK293T cells were stimulated with 200 µg/mL of IGF1 (PHG0078, Thermo Scientific) at different times (0,2,5,7,10 or 30 min) and were lysed at 48 h in 1% Triton X-100 lysis buffer [10 mM Tris-HCl pH 7.4, 5 mM EDTA, 1% Triton X-100, protease inhibitor, phosphatase inhibitor (78446, Thermo Scientific)].

For a rescue experiment, *GIGYF1* KO HEK293T were transiently transfected with 1.5 µg of wild-type, p.L111Rfs*234, p.G174Efs*171 and p.E885* GIGYF1 plasmids. Twenty-four hours after transfection, the cells were stimulated with 200 µg/mL of IGF1 (PHG0078, Thermo Scientific,) at 7min. Cells were lysed in 1% Triton X-100 lysis buffer.

The cortex tissues were obtained from *Gigyf1*$^{f/f}$, cHET and cKO mice at E14.5, then were homogenised in 10 volumes of 1% Triton X-100 lysis buffer (10 mM Tris-HCl pH 7.4, 5 mM

EDTA, 1% Triton X-100, protease inhibitor, phosphatase inhibitor). The homogenates were centrifuged at 10000 g for 15 min at 4℃.

All of the above supernatants were separated by SDS-PAGE and transferred from gels to polyvinylidene difluoride membranes (IPVH15150, Millipore-Sigma). And then blocking for an hour at room temperature and analyzed by western blot using primary antibody overnight at 4℃. Adding the secondary antibody by 1:10000. Protein-antibody complexes were detected with SuperSignal West Femto Maximum Sensitivity Substrate (A38556, Thermo Scientific).

Immunoprecipitation assay. pCAGGS-IRES-GFP-HA-GIGYF1 and pcDNA3.1-3xFlag-IGF-1R were co-transfected with 2 μg of each plasmid in HEK293T cells. After 24 h, cells were lysed in NP40 lysis buffer (50 mM Tris, pH7.4, 150 mM NaCl, 1% NP-40, sodium pyrophosphate, β-glycerophosphate, sodium orthovanadate, sodium fluoride, EDTA) (P0013F, Beyotime Biotechnology) and centrifuged at 8000 g for 5 min at 4℃. The supernatants were subjected to immunoprecipitation of anti-HA immunomagnetic beads (B26201, Bimake) and anti-Flag immunomagnetic beads (B23101, Bimake). The lysates (1-2 mg of protein) were respectively incubated with 10 μL beads overnight at 4℃. After the beads were washed with PBST for three times, proteins were eluted with SDS sample buffer (10 mM Tris, pH 7.8, 3% SDS, 5% glycerol and 0.02% bromophenol blue) and were detected by western blot.

Surface biotinylation assay. Surface biotinylation assay was carried out according to the protocal in Truong, A., et al (38). *GIGYF1* KO HEK293T cells and control HEK293T cells were inoculated into 6 cm dishes for 2 days. After discarding the medium, cells were washed twice with 2 mL PBS/CM (PBS containing 1 mM $MgCl_2$ and 1.3 mM $CaCl_2$), then incubated with fresh-made solution of SulfoNHS-SS-Biotin (PG82077, Thermo Scientific) (0.25 mg/mL) for 30 min at 4℃. 50 mM NH4Cl was added in PBS/CM to stop the reaction at 4 ℃ for 10 min. The cells were

lysated with lysis buffer (0.2% SDS, 1% Triton X-100, 0.5% Deoxycholic acid, 50 mM Tris-HCl, pH 8.0, 150 mM NaCl, protease inhibitors), and then 500 μg biotinylated proteins were purified with NeutrAvidin Agarose (29200, Thermo Scientific) for 1 h at room temperature. The purified biotinylated proteins were incubated in elution buffer (50 mM DTT, 2% SDS, 62.5 mM Tris-HCl, pH 6.8, 10% glycerol) for 1 h at room temperature to remove biotin. The expression of surface IGF-1R was detected by western blot.

Surface biotinylation recycling assay. Surface biotinylation assay was also carried out according to the protocal in Truong, A., et al (38). *GIGYF1* KO and control HEK293T cells were surface labelled with Sulfo-NHS-SS-Biotin (0.25 mg/mL). The labelling reaction was quenched, and then cells were incubated with fresh medium at 37˚C for 30 min to endocytosis. Remaining surface biotin was cleaved with glutathione cleavage buffer (50 mM glutathione, 75 mM NaCl, 10 mM EDTA, 1% BSA, 75 mM NaOH) at 37˚C for 30 min twice. To detect IGF-1R endocytosis, the cells were lysed, and biotinylated proteins were purified with NeutrAvidin Agarose. Cells were incubated with serum-free growth medium for a second time at 37˚C for 30 min to recycle and surface stripped for a second time. Then cells were lysed and incubated with NeutrAvidin Agarose. The beads were washed, proteins were eluted using DTT and then separated by SDS-PAGE. Proteins were immunoblotted by western blot.

Neurosphere culture

The cortical tissues of embryonic mice at E14.5 were isolated. The obtained cortical tissues were mechanically triturated into single cells with Accutase™ (00-4555-56, Thermo Scientific). Wash twice with DMEM plus 10% FBS medium. A neurosphere medium used after the cortex is blown into single cells with a pipette. Cells were plated at a cell density of $3*10^4$-10^5 cells/mL on uncoated 6-well dishes and cultured in DMEM/F12 (11320033, Gibco), B27 supplement

(17504044, Gibco), 10 ng/mL bFGF, and 20 ng/mL EGF (Invitrogen). For the self-renewal analysis of NPCs, primary neurospheres were dissociated with Accutase™ and passaged at a cell density of 100 cell/mL on uncoated 24-well dishes using the same culture conditions as in the primary culture. The size of primary neurospheres was counted after 3 days, 5 days, 7 days of culture.

Statistical analysis. All experiments were performed with a minimum of three independent replicates. Unpaired or paired Student's t test, one-way or two-way ANOVA were performed, where appropriate, to analyse data. All data are presented with mean values and SEM. Differences were considered significant with $p < 0.05$.

Study approval. Written informed consent was obtained from study participants or their parents or legal guardians, in line with local institutional review board (IRB) requirements at the time of collection. The IRB of the Central South University approved this study (#2019-1-23). All animal experiments were complied with all relevant ethical regulations and were approved by the IRB of Central South University (IRB#2019-2-23).

Data and Code Availability

The WES and WGS data used in this study are available from the following resources. The GATK VCF files for SPARK WES and WGS data and SPARK phenotype data used in this study are available through SFARI and available to approved researchers at SFARI Base (accession nos. SFARI_SPARK_WES_p, SFARI_SPARK_WES_1, SFARI_SPARK_WES_2, SFARI_SPARK_WES_3, SFARI_SPARK_WGS_1, SFARI_SPARK_WGS_2, SFARI_SPARK_WGS_3). All GATK VCF files for SSC WGS data and SSC phenotype data are available by request from SFARI Base (accession no. SFARI_SSC_WGS). All software used in this study is publicly available.

Acknowledgements

We thank T. Brown for assistance in editing this manuscript. We thank all the families in SPARK, the SPARK clinical sites and SPARK staff. We thank all the families at the participating SSC sites, as well as the principal investigators (A. Beaudet, R. Bernier, J. Constantino, E. Cook, E. Fombonne, D. Geschwind, R. Goin-Kochel, E. Hanson, D. Grice, A. Klin, D. Ledbetter, C. Lord, C. Martin, D. Martin, R. Maxim, J. Miles, O. Ousley, K. Pelphrey, B. Peterson, J. Piggot, C. Saulnier, M. State, W. Stone, J. Sutcliffe, C. Walsh, Z. Warren and E. Wijsman). We appreciate obtaining access to the phenotypic and genetic data on SFARI Base. Approved researchers can obtain the SSC population dataset described in this study (https://www.sfari.org/ resource/simons-simplex-collection/) and the SPARK population dataset described in this study (https://www.sfari.org/resource/spark/) by applying at https://base.sfari. org. We are grateful to all the other families participating this study. We thank Jiada Li and other colleagues from the QinXueHaoWen forum for their critical comments. We thank Matthew Page and Martin Armstrong for their technical assistance. This work was supported, in part, by grants from the National Natural Science Foundation of China (no. 81871079 to H.G.; no. 8173000779, and no. 82130043 to K.X.), National Brain Science and Brain-like Research of China (no. 2021ZD0201704 to H.G.); National Key Research and Development Program of China (no. 2021YFA0805200 to Z.H. and J.T.); Hunan Provincial grants (no. 2021JJ10070, no. 2019RS2005, no. 2019SK1015 and no. 2021DK2001 to H.G.), and the National Institutes of Health (NIH R01MH101221 to E.E.E.). E.E.E. is an investigator of the Howard Hughes Medical Institute.

Author Contributions

H.G., G.C., B.Y., S.T., J.T., and K.X. designed and conceived this study. S.T and H.G. analyzed and interpreted the genotype and phenotype data. G.C. and B.Y. performed the mouse behavioral

and neurogenesis analysis. B.Y., G.C., and J.T. designed the cell biology, histology, and biochemistry studies; and analyzed the data. E.E.E., J.T., X.J., Q.Z., X.Z., Q.J., Y.Hua., Y.Han., Q.P., Z.H., and L.Y. helped with data interpretation. H.G. and K.X. supervised the work. G.C., B.Y., S.T., H.G., J.T., E.E.E., and K.X. wrote and revised the manuscript. Other authors including A.F., S.A, S.D.K, R.A.B, R.K.E, E.C.K, L.L.P.R, F.K., M.L.S.F.F, D.M., D.B., R.E.S, J.S., S.M., C.M.E.I.A, M.I., and S.M.K., contributed and interpreted the genetic and clinical data recruited from international collaborative network. All authors commented on the manuscript and approved the final manuscript. G.C., B.Y., S.T. and J.T. made equally important contributions from four different angles of this study and are thus considered as co–first authors.

Conflict of interest

E.E.E. is on the Scientific Advisory Board (SAB) of VariantBio, Inc. All other authors have declared that not conflict of interest exist.

References

1. Lord C, Brugha TS, Charman T, Cusack J, Dumas G, Frazier T, et al. Autism spectrum disorder. *Nat Rev Dis Primers.* 2020;6(1):5.
2. Coe BP, Stessman HAF, Sulovari A, Geisheker MR, Bakken TE, Lake AM, et al. Neurodevelopmental disease genes implicated by de novo mutation and copy number variation morbidity. *Nat Genet.* 2019;51(1):106-16.
3. Kaplanis J, Samocha KE, Wiel L, Zhang Z, Arvai KJ, Eberhardt RY, et al. Evidence for 28 genetic disorders discovered by combining healthcare and research data. *Nature.* 2020;586(7831):757-62.
4. Giovannone B, Lee E, Laviola L, Giorgino F, Cleveland KA, and Smith RJ. Two novel proteins that are linked to insulin-like growth factor (IGF-I) receptors by the Grb10 adapter and modulate IGF-I signaling. *J Biol Chem.* 2003;278(34):31564-73.
5. Iossifov I, O'Roak BJ, Sanders SJ, Ronemus M, Krumm N, Levy D, et al. The contribution of de novo coding mutations to autism spectrum disorder. *Nature.* 2014;515(7526):216-21.
6. Krumm N, Turner TN, Baker C, Vives L, Mohajeri K, Witherspoon K, et al. Excess of rare, inherited truncating mutations in autism. *Nat Genet.* 2015;47(6):582-8.
7. Satterstrom FK, Kosmicki JA, Wang J, Breen MS, De Rubeis S, An JY, et al. Large-Scale Exome Sequencing Study Implicates Both Developmental and Functional Changes in the Neurobiology of Autism. *Cell.* 2020;180(3):568-84 e23.
8. pfeliciano@simonsfoundation.org SCEa, and Consortium S. SPARK: A US Cohort of 50,000 Families to Accelerate Autism Research. *Neuron.* 2018;97(3):488-93.

9. Fischbach GD, and Lord C. The Simons Simplex Collection: a resource for identification of autism genetic risk factors. *Neuron.* 2010;68(2):192-5.

10. Sobreira N, Schiettecatte F, Valle D, and Hamosh A. GeneMatcher: a matching tool for connecting investigators with an interest in the same gene. *Hum Mutat.* 2015;36(10):928-30.

11. Sanders SJ, He X, Willsey AJ, Ercan-Sencicek AG, Samocha KE, Cicek AE, et al. Insights into Autism Spectrum Disorder Genomic Architecture and Biology from 71 Risk Loci. *Neuron.* 2015;87(6):1215-33.

12. Peca J, Feliciano C, Ting JT, Wang W, Wells MF, Venkatraman TN, et al. Shank3 mutant mice display autistic-like behaviours and striatal dysfunction. *Nature.* 2011;472(7344):437-42.

13. de la Torre-Ubieta L, Won H, Stein JL, and Geschwind DH. Advancing the understanding of autism disease mechanisms through genetics. *Nat Med.* 2016;22(4):345-61.

14. Packer A. Neocortical neurogenesis and the etiology of autism spectrum disorder. *Neurosci Biobehav Rev.* 2016;64:185-95.

15. Tan X, and Shi SH. Neocortical neurogenesis and neuronal migration. *Wiley Interdiscip Rev Dev Biol.* 2013;2(4):443-59.

16. Kwan KY, Sestan N, and Anton ES. Transcriptional co-regulation of neuronal migration and laminar identity in the neocortex. *Development.* 2012;139(9):1535-46.

17. Dufresne AM, and Smith RJ. The adapter protein GRB10 is an endogenous negative regulator of insulin-like growth factor signaling. *Endocrinology.* 2005;146(10):4399-409.

18. Shelton JG, Steelman LS, White ER, and McCubrey JA. Synergy between PI3K/Akt and Raf/MEK/ERK pathways in IGF-1R mediated cell cycle progression and prevention of apoptosis in hematopoietic cells. *Cell Cycle.* 2004;3(3):372-9.

19. Zhou T, Ma Y, Tang J, Guo F, Dong M, and Wei Q. Modulation of IGF1R Signaling Pathway by GIGYF1 in High Glucose-Induced SHSY-5Y Cells. *DNA Cell Biol.* 2018;37(12):1044-54.

20. Crudden C, Song D, Cismas S, Trocme E, Pasca S, Calin GA, et al. Below the Surface: IGF-1R Therapeutic Targeting and Its Endocytic Journey. *Cells.* 2019;8(10).

21. Rieger L, and O'Connor R. Controlled Signaling-Insulin-Like Growth Factor Receptor Endocytosis and Presence at Intracellular Compartments. *Front Endocrinol (Lausanne).* 2020;11:620013.

22. Chambard JC, Lefloch R, Pouyssegur J, and Lenormand P. ERK implication in cell cycle regulation. *Biochim Biophys Acta.* 2007;1773(8):1299-310.

23. Villanueva J, Yung Y, Walker JL, and Assoian RK. ERK activity and G1 phase progression: identifying dispensable versus essential activities and primary versus secondary targets. *Mol Biol Cell.* 2007;18(4):1457-63.

24. McDonald MJ, Yu YH, Guo JF, Chong SY, Kao CF, and Leu JY. Mutation at a distance caused by homopolymeric guanine repeats in Saccharomyces cerevisiae. *Sci Adv.* 2016;2(5):e1501033.

25. Pucilowska J, Puzerey PA, Karlo JC, Galan RF, and Landreth GE. Disrupted ERK signaling during cortical development leads to abnormal progenitor proliferation, neuronal and network excitability and behavior, modeling human neuro-cardio-facial-cutaneous and related syndromes. *J Neurosci.* 2012;32(25):8663-77.

26. Lavoie H, Gagnon J, and Therrien M. ERK signalling: a master regulator of cell behaviour, life and fate. *Nat Rev Mol Cell Biol.* 2020;21(10):607-32.

27. Ward ES, Martinez C, Vaccaro C, Zhou J, Tang Q, and Ober RJ. From sorting endosomes to exocytosis: association of Rab4 and Rab11 GTPases with the Fc receptor, FcRn, during recycling. *Mol Biol Cell.* 2005;16(4):2028-38.

28. Li H. A statistical framework for SNP calling, mutation discovery, association mapping and population genetical parameter estimation from sequencing data. *Bioinformatics.* 2011;27(21):2987-93.

29. Danecek P, Auton A, Abecasis G, Albers CA, Banks E, DePristo MA, et al. The variant call format and VCFtools. *Bioinformatics.* 2011;27(15):2156-8.

30. Van der Auwera GA, Carneiro MO, Hartl C, Poplin R, Del Angel G, Levy-Moonshine A, et al. From FastQ data to high confidence variant calls: the Genome Analysis Toolkit best practices pipeline. *Curr Protoc Bioinformatics.* 2013;43:11 0 1- 0 33.

31. Karczewski KJ, Francioli LC, Tiao G, Cummings BB, Alfoldi J, Wang Q, et al. The mutational constraint spectrum quantified from variation in 141,456 humans. *Nature.* 2020;581(7809):434-43.

32. Thorvaldsdottir H, Robinson JT, and Mesirov JP. Integrative Genomics Viewer (IGV): high-performance genomics data visualization and exploration. *Brief Bioinform.* 2013;14(2):178-92.

33. Wang K, Li M, and Hakonarson H. ANNOVAR: functional annotation of genetic variants from high-throughput sequencing data. *Nucleic Acids Res.* 2010;38(16):e164.

34. Ware JS, Samocha KE, Homsy J, and Daly MJ. Interpreting de novo Variation in Human Disease Using denovolyzeR. *Curr Protoc Hum Genet.* 2015;87:7 25 1-7 15.

35. O'Roak BJ, Vives L, Fu W, Egertson JD, Stanaway IB, Phelps IG, et al. Multiplex targeted sequencing identifies recurrently mutated genes in autism spectrum disorders. *Science.* 2012;338(6114):1619-22.

36. He Z, O'Roak BJ, Smith JD, Wang G, Hooker S, Santos-Cortez RL, et al. Rare-variant extensions of the transmission disequilibrium test: application to autism exome sequence data. *Am J Hum Genet.* 2014;94(1):33-46.

37. Houlihan SL, and Feng Y. The scaffold protein Nde1 safeguards the brain genome during S phase of early neural progenitor differentiation. *Elife.* 2014;3:e03297.

38. Truong A, Yip C, Paye A, Blacher S, Munaut C, Deroanne C, et al. Dynamics of internalization and recycling of the prometastatic membrane type 4 matrix metalloproteinase (MT4-MMP) in breast cancer cells. *FEBS J.* 2016;283(4):704-22.

Figure 1

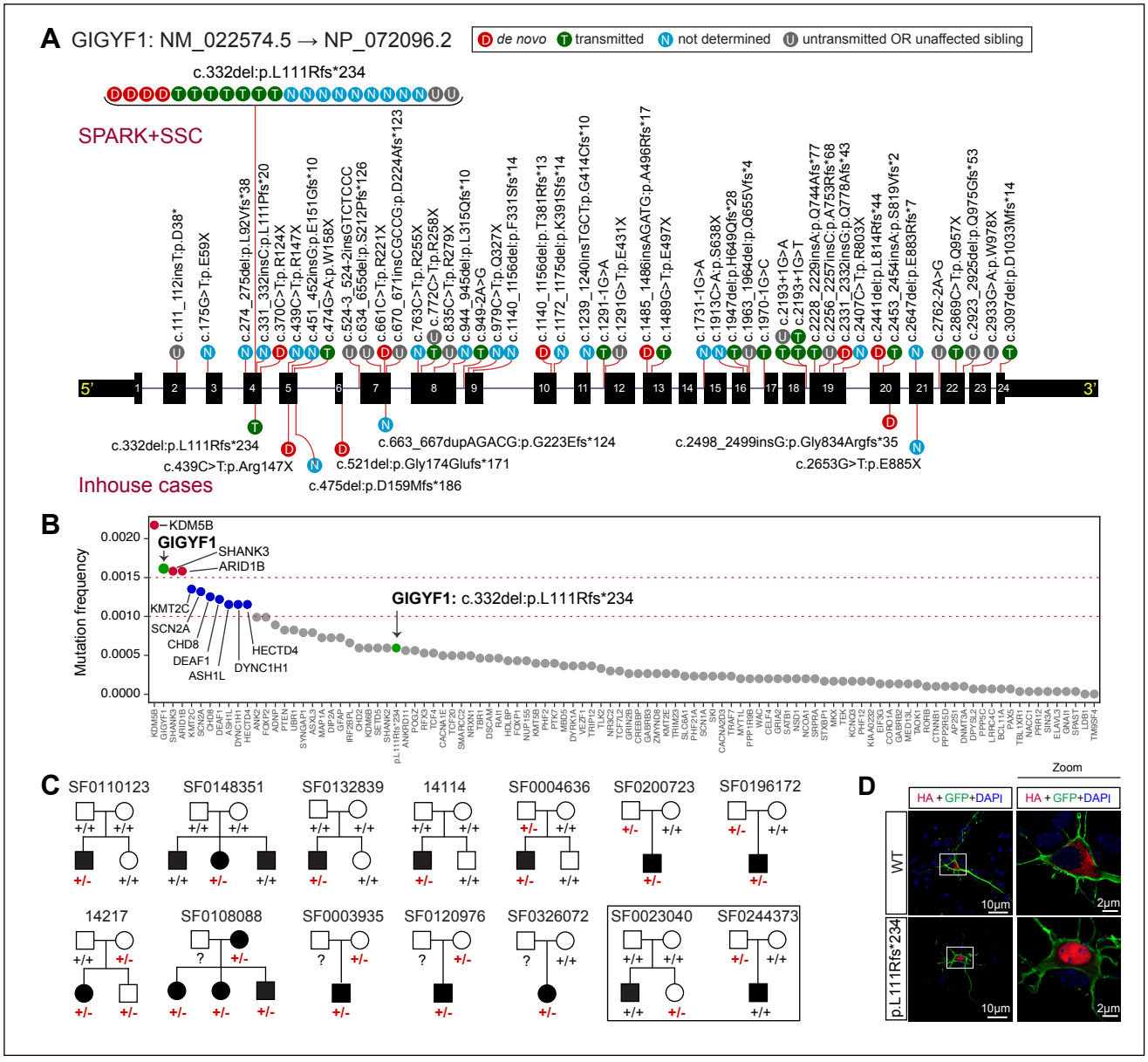
A
GIGYF1: NM_022574.5 → NP_072096.2
de novo
transmitted
not determined
untransmitted OR unaffected sibling
c.332del:p.L111Rfs*234
SPARK+SSC
c.111_112insT:p.D38*
c.175G>T:p.E59X
c.274_275del:p.L92Vfs*38
c.331_332insC:p.L111Pfs*20
c.370C>T:p.R124X
c.439C>T:p.R147X
c.451_452insG:p.E151Gfs*10
c.474G>A:p.W158X
c.524-3_524-2insGTCTCCC
c.634_655del:p.S212Pfs*126
c.661C>T:p.R221X
c.670_671insCGCCG:p.D224Afs*123
c.763C>T:p.R255X
c.772C>T:p.R258X
c.835C>T:p.R279X
c.944_945del:p.L315Qfs*10
c.949-2A>G
c.979C>T:p.Q327X
c.1140_1156del:p.F331Sfs*14
c.1140_1156del:p.T381Rfs*13
c.1172_1175del:p.K391Sfs*14
c.1239_1240insTGCT:p.G414Cfs*10
c.1291-1G>A
c.1291G>T:p.E431X
c.1485_1486insAGATG:p.A496Rfs*17
c.1489G>T:p.E497X
c.1731-1G>A
c.1913C>A:p.S638X
c.1947del:p.H649Qfs*28
c.1963_1964del:p.Q655Vfs*4
c.1970-1G>C
c.2193+1G>A
c.2193+1G>T
c.2228_2229insA:p.Q744Afs*77
c.2256_2257insC:p.A753Rfs*68
c.2331_2332insG:p.Q778Afs*43
c.2407C>T:p.R803X
c.2441del:p.L814Rfs*44
c.2453_2454insA:p.S819Vfs*2
c.2647del:p.E883Rfs*7
c.2762-2A>G
c.2869C>T:p.Q957X
c.2923_2925del:p.Q975Gfs*53
c.2933G>A:p.W978X
c.3097del:p.D1033Mfs*14
5'
3'
c.332del:p.L111Rfs*234
c.439C>T:p.Arg147X
c.475del:p.D159Mfs*186
c.521del:p.Gly174Glufs*171
c.663_667dupAGACG:p.G223Efs*124
c.2498_2499insG:p.Gly834Argfs*35
c.2653G>T:p.E885X
Inhouse cases
B
Mutation frequency
0.0020
0.0015
0.0010
0.0005
0.0000
KDM5B
GIGYF1
SHANK3
ARID1B
KMT2C
SCN2A
CHD8
DEAF1
ASH1L
HECTD4
DYNC1H1
GIGYF1: c.332del:p.L111Rfs*234
C
SF0110123
SF0148351
SF0132839
14114
SF0004636
SF0200723
SF0196172
14217
SF0108088
SF0003935
SF0120976
SF0326072
SF0023040
SF0244373
+/+
+/-
?
D
Zoom
HA + GFP+DAPI
WT
p.L111Rfs*234
10μm
2μm

Figure Legends

Figure 1. Pattern, distribution, and inheritance of *GIGYF1* heterozygous LGD mutations in human. (**A**) Mutation pattern of *GIGYF1* LGD variants identified in SPARK/SSC cohorts (above) and through GeneMatcher (below) on a gene model. (**B**) Ranked mutation frequency of LGD variants in 102 high-confidence genes identified in Satterstrom, *et al*. (7). (**C**) Pedigrees with the recurrent variant p.L111Rfs*234 identified in SPARK and SSC cohorts (+/+ wild-type, +/- heterozygous). Families with untransmitted or *de novo GIGFY1* LGD variants in unaffected siblings are squared. Solid circles or squares represent individuals with ASD diagnosis. (**D**) The recurrent LGD site p.L111Rfs*234 shows abnormal localization in mouse primary cultured neurons. The wild-type (WT) plasmid is mainly located in the cytoplasm; however, the mutant is absolutely located in the nuclei. Scale bars represent 10 μm. Scale bars of zoom area represent 2 μm.

Figure 2

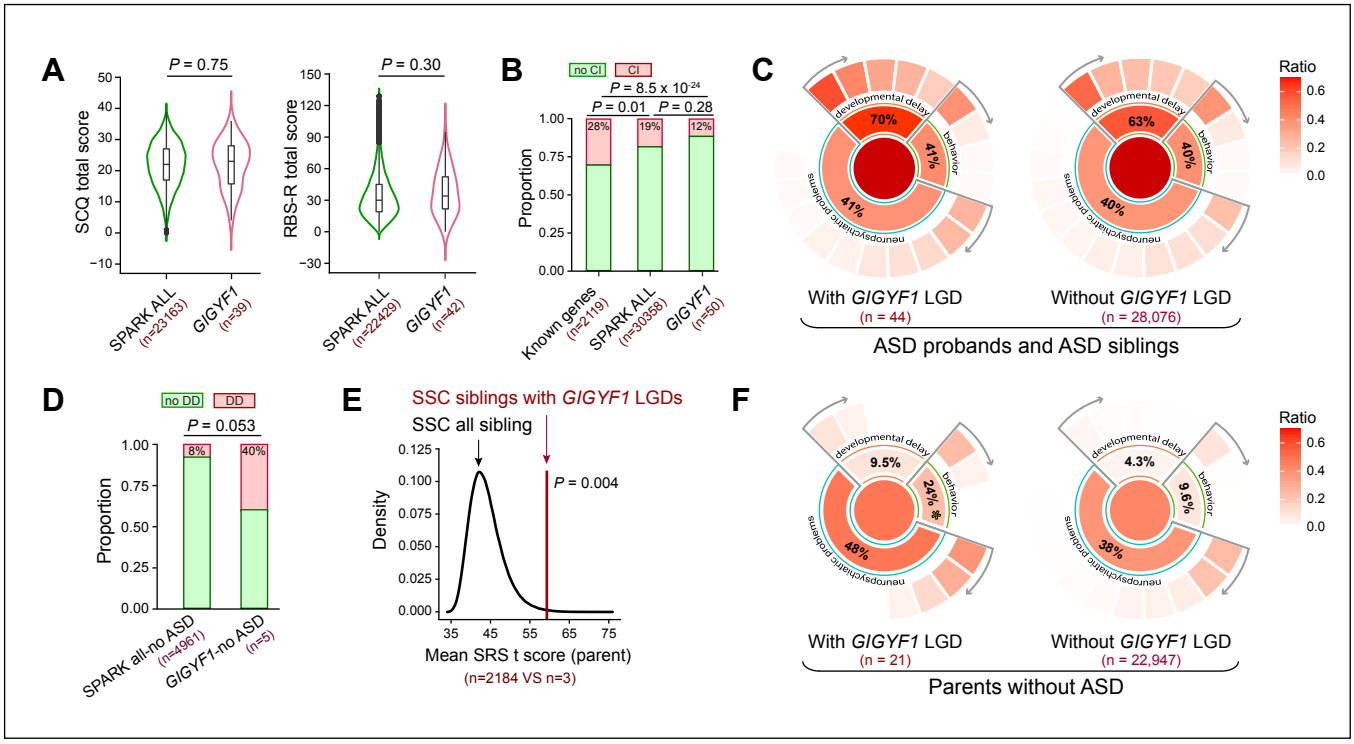
A
P = 0.75
SCQ total score
SPARK ALL (n=23163)
GIGYF1 (n=39)
P = 0.30
RBS-R total score
SPARK ALL (n=22429)
GIGYF1 (n=42)
B
no CI
CI
P = 8.5 x 10-24
P = 0.01
P = 0.28
Proportion
28%
19%
12%
Known genes (n=2119)
SPARK ALL (n=30358)
GIGYF1 (n=50)
C
developmental delay
behavior
neuropsychiatric problems
70%
41%
41%
63%
40%
40%
Ratio
With GIGYF1 LGD (n = 44)
Without GIGYF1 LGD (n = 28,076)
ASD probands and ASD siblings
D
no DD
DD
P = 0.053
Proportion
8%
40%
SPARK all-no ASD (n=4961)
GIGYF1-no ASD (n=5)
E
SSC siblings with GIGYF1 LGDs
SSC all sibling
P = 0.004
Density
Mean SRS t score (parent)
(n=2184 VS n=3)
F
9.5%
24%
48%
4.3%
9.6%
38%
With GIGYF1 LGD (n = 21)
Without GIGYF1 LGD (n = 22,947)
Parents without ASD

Figure 2. Phenotypic correlation of *GIGYF1* heterozygous LGD mutations. (**A**) Comparison of the Social Communication Questionnaire (SCQ) and Repetitive Behaviors Scale–Revised (RBS-R) scores between ASD children with *GIGYF1* LGD variants and all SPARK ASD children. (**B**) Comparison of cognitive impairment (CI) occurrence rate among ASD children with *GIGYF1* LGD variants, ASD children with LGD variants in known high-confidence genes, and all SPARK ASD children. (**C**) Comparison of the frequency of behavior problems, developmental delays, and neuropsychiatric problems between ASD children with and without *GIGYF1* LGD variants. The details of specific phenotype items for each phenotype group in the plot are described in Table S9. (**D**) Comparison of developmental delay occurrence rate among non-ASD children with *GIGYF1* LGD variants and all SPARK non-ASD children. (**E**) Down-sampling analysis of SRS t score in siblings without ASD from SSC cohort. (**F**) Comparison of the frequency of behavior problems, developmental delay, and neuropsychiatric problems between non-ASD parents with and without *GIGYF1* LGD variants. The details of specific phenotype items for each phenotype group in the plot are described in Table S9.

Figure 3

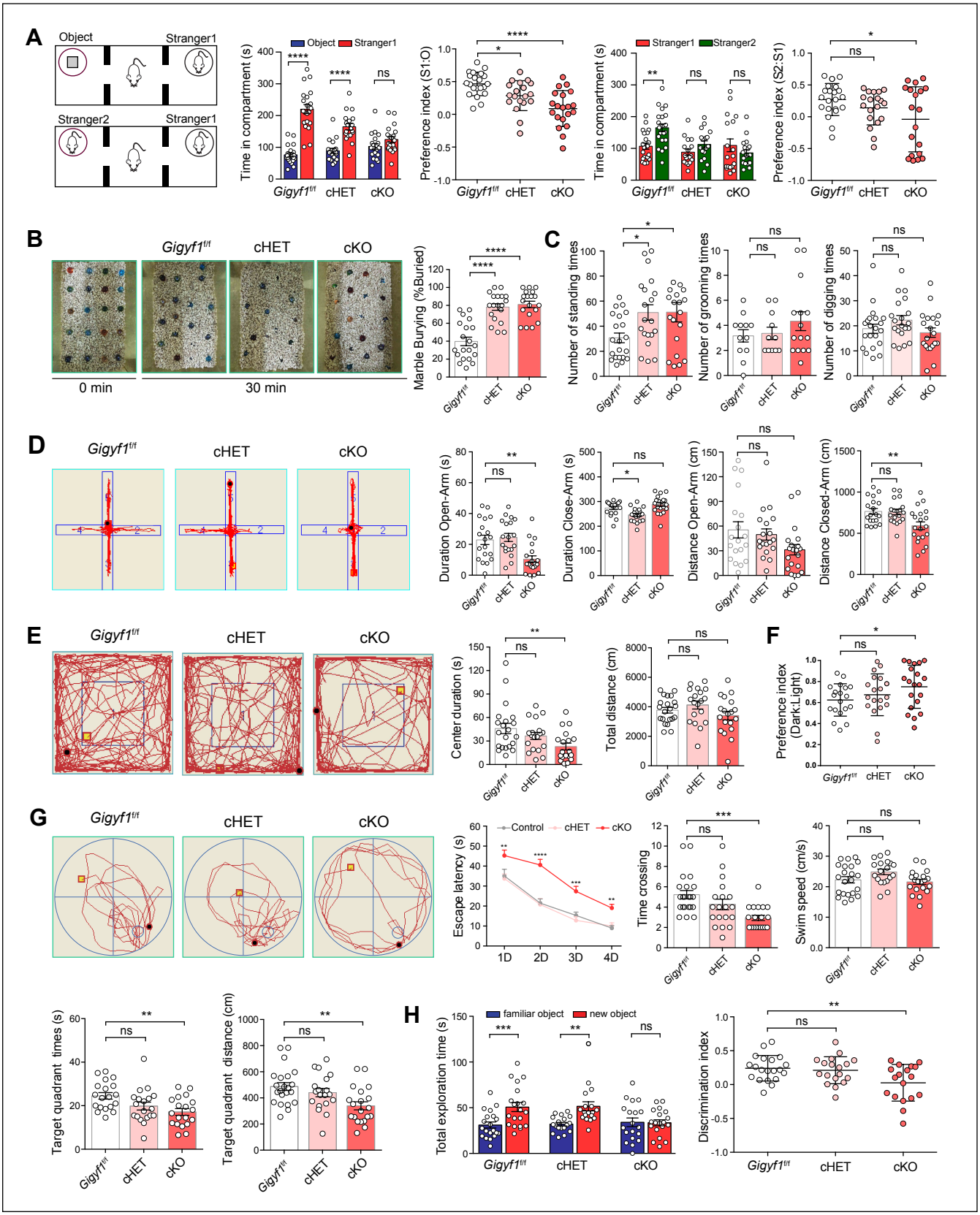
A
Object
Stranger1
Stranger2
Stranger1
Object
Stranger1
Time in compartment (s)
Gigyf1f/f
cHET
cKO
Preference index (S1:O)
Stranger1
Stranger2
Time in compartment (s)
Preference index (S2:S1)
B
Gigyf1f/f
cHET
cKO
0 min
30 min
Marble Burying (%Buried)
C
Number of standing times
Number of grooming times
Number of digging times
D
Gigyf1f/f
cHET
cKO
Duration Open-Arm (s)
Duration Close-Arm (s)
Distance Open-Arm (cm)
Distance Closed-Arm (cm)
E
Gigyf1f/f
cHET
cKO
Center duration (s)
Total distance (cm)
F
Preference index (Dark:Light)
G
Gigyf1f/f
cHET
cKO
Control
cHET
cKO
Escape latency (s)
1D
2D
3D
4D
Time crossing
Swim speed (cm/s)
Target quadrant times (s)
Target quadrant distance (cm)
H
familiar object
new object
Total exploration time (s)
Discrimination index

Figure 3. *Gigyf1* haploinsufficiency and knockout in mouse developing brain results in autistic-like behaviors. (**A**) Three-chamber test.The time spent with object (O), stranger 1 (S1) and stranger 2 (S2) was compared. The preference indexes were compared. n = 21 (*Gigyf1*$^{f/f}$), 19 (cHET), 20 (cKO). Statistic data were analyzed using one-way ANOVA and two-tailed Student's T test. (**B**) Marbles bury test. The percentage of buried marbles was compared. Statistic data were analyzed using one-way ANOVA. (**C**) Digging, rearing, and grooming test. The numbers of digging, rearing, and grooming were compared. n = 20 (*Gigyf1*$^{f/f}$), 19 (cHET), 19 (cKO). Statistic data were analyzed using one-way ANOVA. (**D**) Elevated plus maze test. The time and the total distance in open and closed arms were compared. n = 19 (*Gigyf1*$^{f/f}$), 19 (cHET), 20 (cKO). Statistic data were analyzed using one-way ANOVA. (**E**) Open field test. The total distance and center duration were compared. n = 21 (*Gigyf1*$^{f/f}$), 19 (cHET), 19 (cKO). Statistic data were analyzed using one-way ANOVA. (**F**) Light and dark test. The preference indexes to dark box were compared. n = 19 (*Gigyf1*$^{f/f}$), 19 (cHET), 20 (cKO). Statistic data were analyzed using one-way ANOVA. (**G**) Morris water-maze test. The escape latency in the learning phase, the number of exact crossings over the former hidden platform in the probe phase, the swim speed, and the time and distance in the target quadrant in the probe phase were compared. n = 22 (*Gigyf1*$^{f/f}$), 19 (cHET), 20 (cKO). Statistic data were analyzed using one-way and two-way ANOVA. (**H**) Novel-object recognition test. Total exploration time and discrimination index were compared. n = 20 (*Gigyf1*$^{f/f}$), 18 (cHET), 19 (cKO). Statistic data were analyzed using one-way ANOVA and two-tailed Student's T test. All data are represented as mean ± SEM. *p<0.05, **p<0.01, ***p<0.001, ****P<0.0001, ns, not significant.

Figure 4

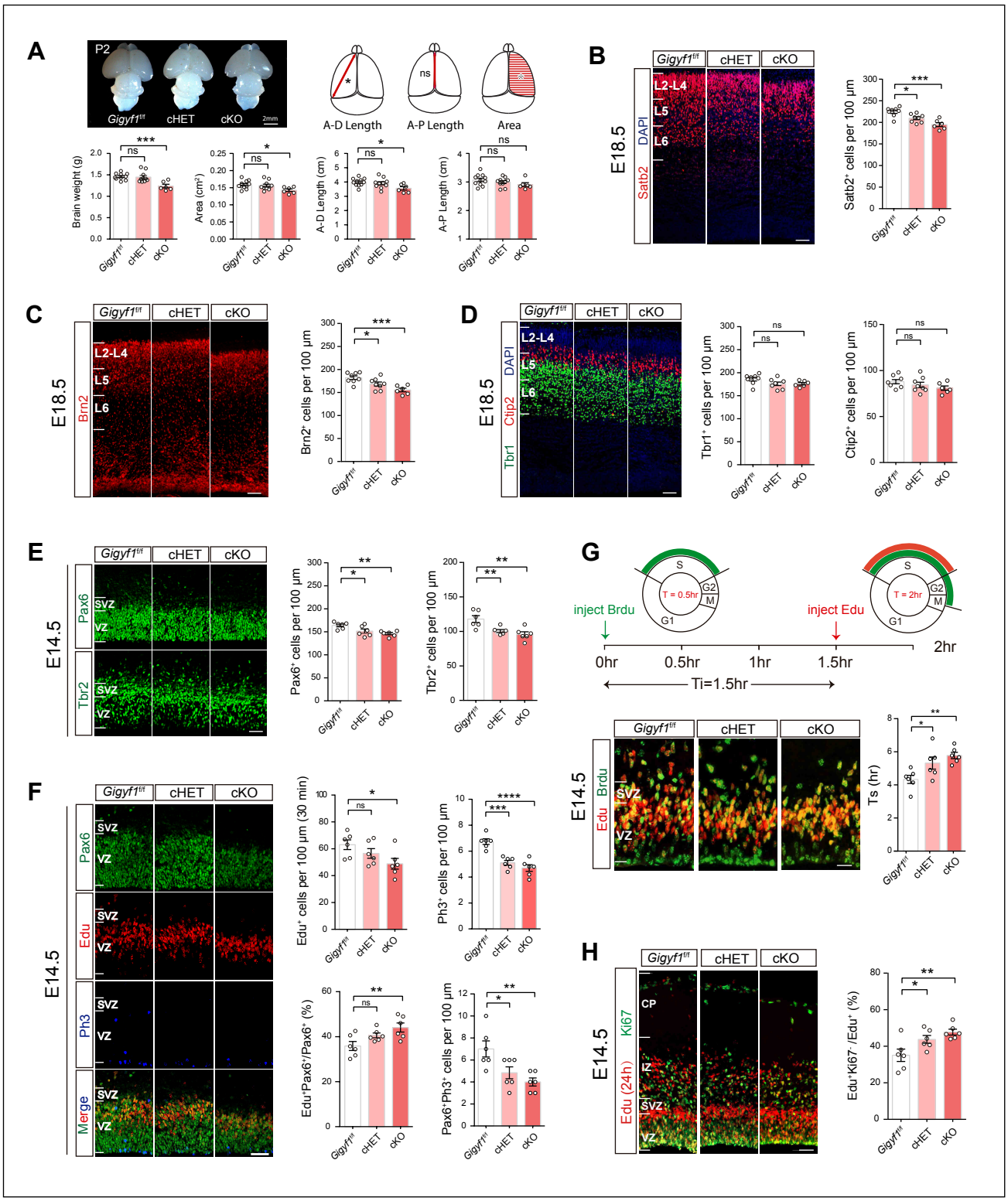
A
P2
Gigyf1f/f
cHET
cKO
2mm
A-D Length
A-P Length
Area
Brain weight (g)
Area (cm²)
A-D Length (cm)
A-P Length (cm)
B
E18.5
L2-L4
L5
L6
Satb2
DAPI
Satb2⁺ cells per 100 μm
C
Brn2
Brn2⁺ cells per 100 μm
D
Ctip2
Tbr1
Tbr1⁺ cells per 100 μm
Ctip2⁺ cells per 100 μm
E
E14.5
Pax6
Tbr2
SVZ
VZ
Pax6⁺ cells per 100 μm
Tbr2⁺ cells per 100 μm
F
Edu
Ph3
Merge
Edu⁺ cells per 100 μm (30 min)
Ph3⁺ cells per 100 μm
Edu⁺Pax6⁺/Pax6⁺ (%)
Pax6⁺Ph3⁺ cells per 100 μm
G
inject Brdu
inject Edu
T = 0.5hr
T = 2hr
S
G1
G2
M
0hr
0.5hr
1hr
1.5hr
2hr
Ti=1.5hr
Brdu
Ts (hr)
H
Ki67
Edu (24h)
CP
IZ
Edu⁺Ki67⁺/Edu⁺ (%)

Figure 4. *Gigyf1* disruption in the developing brain disturbs neurogenesis. (**A**) Quantitative comparison of brain weight, cortical A-D length, A-P length and area in *Gigyf1*$^{f/f}$ (n = 11), cHET (n = 10), and cKO (n = 6) mice at P2. (**B**) Littermate cortices stained with Satb2 from *Gigyf1*$^{f/f}$ (n = 4), cHET (n = 4), and cKO (n = 3) mice at E18.5. Satb2^{+} cells per 100 μm of apical surface in L2-L4 were compared. (**C**) Littermate cortices stained with Brn2 from *Gigyf1*$^{f/f}$ (n = 4), cHET (n = 4), and cKO (n = 3) mice at E18.5. Brn2^{+} cells per 100 μm of apical surface in L2-L4 were compared. (**D**) Littermate cortices stained with Tbr1 and Ctip2 from *Gigyf1*$^{f/f}$ (n = 4), cHET (n = 4), and cKO (n = 3) mice at E18.5. Ctip2^{+} cells and Tbr1^{+} cells per 100 μm in L5 and L6 were compared. (**E**) Comparison of Pax6^{+} RGC (VZ) and Tbr2^{+} IPC (SVZ) populations per 100 μm of apical surface in *Gigyf1*$^{f/f}$ (n = 3), cHET (n = 3), and cKO (n = 3) mice at E14.5. (**F**) Comparison of Edu^{+} (SVZ) population, Ph3^{+} and Pax6^{+}Ph3^{+} (VZ) population, Pax6^{+}Edu^{+}/Pax6^{+} proportion of apical surface from *Gigyf1*$^{f/f}$ (n = 3), cHET (n = 3), and cKO (n = 3) mice at E14.5. (**G**) Ki67 and Edu antibodies after 24h Edu pulse at E13.5. All cells that exited the cell cycles (Edu^{+}/Ki67^{-}) were counted. The percentage of total Edu^{+} cells evaluated 24h post-injection was analyzed. (**H**) S phase sequential labeling analysis of NPCs. EdU-Brdu double-stained cortical sections at E14.5 are shown. S phase durations were calculated (Ts=Ti/(Lcells/Scells)) and compared. All statistics were performed by one-way ANOVA. Scale bars represent 50 μm. All data are represented as mean ± SEM. *p<0.05, **p<0.01, ***p<0.001, ****P<0.0001, ns, not significant.

Figure 5

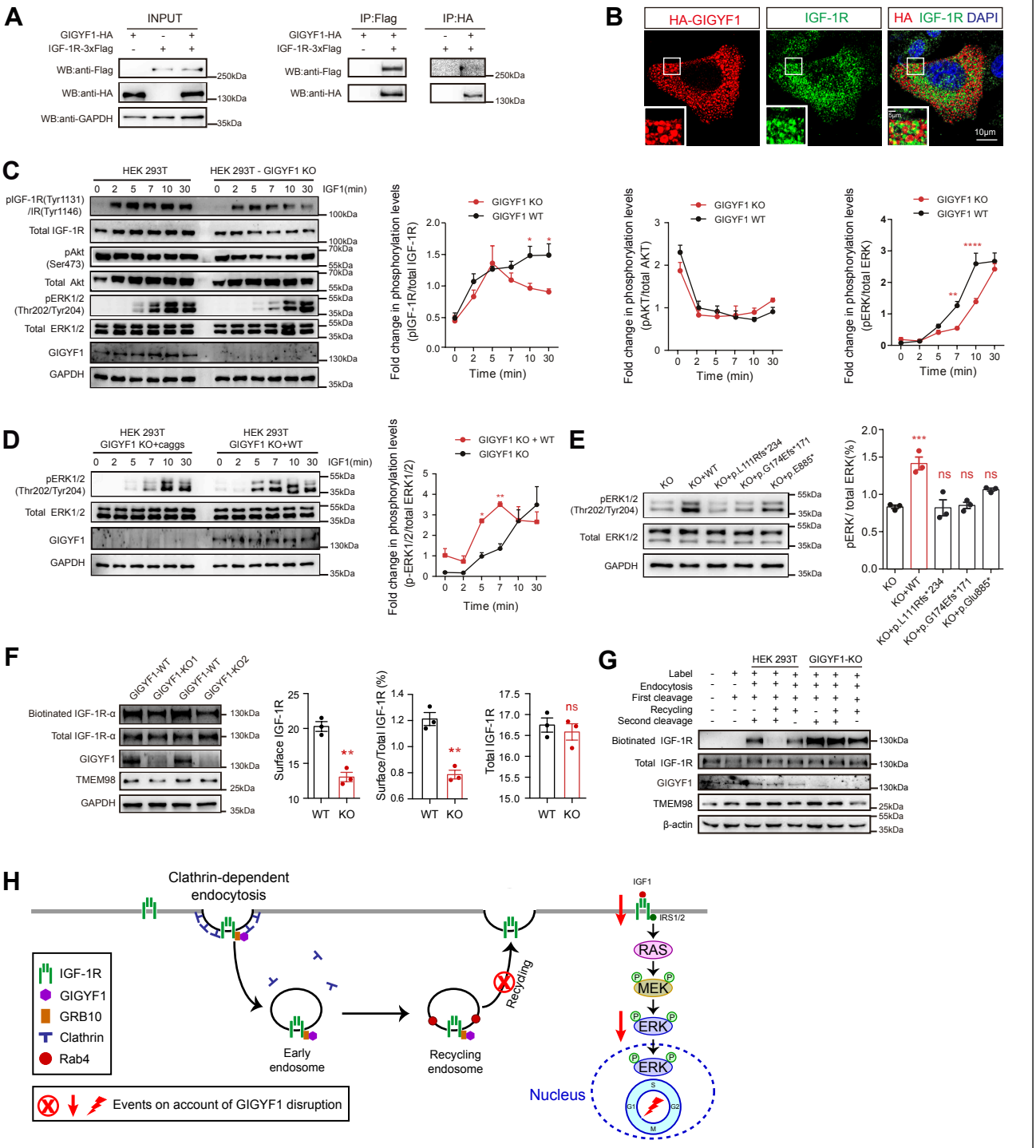
A
INPUT
IP:Flag
IP:HA
GIGYF1-HA
IGF-1R-3xFlag
WB:anti-Flag
WB:anti-HA
WB:anti-GAPDH
250kDa
130kDa
35kDa
B
HA-GIGYF1
IGF-1R
HA IGF-1R DAPI
10μm
C
HEK 293T
HEK 293T - GIGYF1 KO
IGF1(min)
pIGF-1R(Tyr1131) /IR(Tyr1146)
Total IGF-1R
pAkt (Ser473)
Total Akt
pERK1/2 (Thr202/Tyr204)
Total ERK1/2
GIGYF1
GAPDH
Fold change in phosphorylation levels (pIGF-1R/total IGF-1R)
Fold change in phosphorylation levels (pAKT/total AKT)
Fold change in phosphorylation levels (pERK/total ERK)
GIGYF1 KO
GIGYF1 WT
Time (min)
D
HEK 293T GIGYF1 KO+caggs
HEK 293T GIGYF1 KO+WT
Fold change in phosphorylation levels (p-ERK1/2/total ERK1/2)
GIGYF1 KO + WT
E
KO
KO+WT
KO+p.L111Rfs*234
KO+p.G174Efs*171
KO+p.E885*
pERK/ total ERK(%)
ns
F
GIGYF1-WT
GIGYF1-KO1
GIGYF1-KO2
Biotinated IGF-1R-α
Total IGF-1R-α
TMEM98
Surface IGF-1R
Surface/Total IGF-1R (%)
Total IGF-1R
WT
KO
G
HEK 293T
GIGYF1-KO
Label
Endocytosis
First cleavage
Recycling
Second cleavage
Biotinated IGF-1R
Total IGF-1R
GIGYF1
TMEM98
β-actin
H
Clathrin-dependent endocytosis
IGF1
IRS1/2
RAS
MEK
ERK
Nucleus
IGF-1R
GIGYF1
GRB10
Clathrin
Rab4
Early endosome
Recycling endosome
Recycling
Events on account of GIGYF1 disruption

Figure 5. *GIGYF1* knockout disrupts IGF-1R/ERK pathway by regulation of IGF-1R recycling. (**A**) Co-immunoprecipitation assay for GIGYF1 and IGF-1R in HEK293T cells. (**B**) Double immunofluorescence of GIGYF1 and IGF-1R in HeLa cells. Scale bars represent 10 μm. Scale bars of insets represent 5 μm. (**C**) Immunoblots of the whole cell lysate showing levels of pIGF-1R, IGF-1R, pERK1/2, ERK1/2, pAkt, and Akt at different duration of IGF-1 stimulation. Statistic data were analyzed using two-way ANOVA. (**D**) Immunoblots of the whole-cell lysates showing levels of pERK1/2, ERK1/2 in HEK293T *GIGYF1* KO cells expressing mock empty vector (pCAGGS-IRES-GFP) or HA-GIGYF1. The relative levels of pERK1/2 to ERK1/2 were quantified by densitometry and analyzed using two-way ANOVA. (**E**) Immunoblot of pERK1/2 and ERK1/2 in the whole-cell lysates at 7 min of IGF-1 stimulation. Statistic data were analyzed using one-way ANOVA. (**F**) Immunoblots of biotin-labelled IGF-1R, total IGF-1R and TMEM98. Total IGF-1R-α levels of unbiotinylated cells were determined. The protein levels of surface IGF-1R, surface IGF-1R/total IGF-1R, and total IGF-1R were quantified by densitometry from three biological replicates. Statistic data were analyzed using two-tailed Student's T-test. (**G**) Immunoblots of biotin-labelled IGF-1R and total IGF-1R at different conditions in surface biotinylation recycling assay. *GIGYF1* KO HEK293T cells and control HEK293T cells (lanes 2–8) were surface labelled with sulfo-NHS-S-S-biotin. Cells (lanes 3-8) were incubated to endocytosis. Remaining surface biotin was cleaved with glutathione cleavage buffer (lanes 2-8). Cells were incubated for a second time to recycle (lanes 4-5 and 7-8), and then, the surface biotin were stripped for a second time (lanes 3-4 and 6-7). Lanes 5 and 8 were incubated to recycle without a second cleavage. (**H**) Working model of GIGYF1 regulation of IGF-1R/ERK pathway. All data are represented as mean ± SEM. *P<0.05, **P<0.01, ****P<0.0001, ns, not significant.

Figure 6

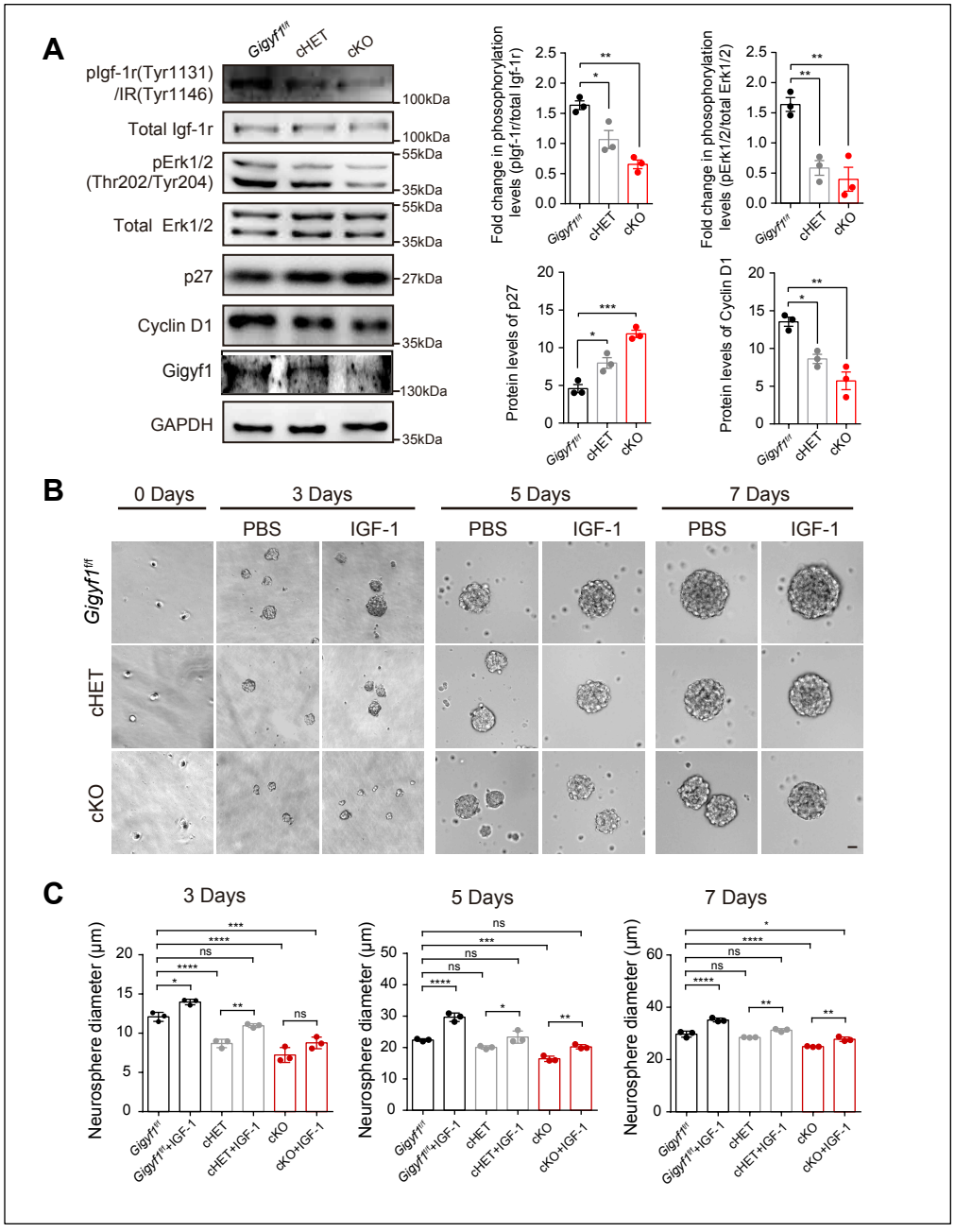
A
Gigyf1f/f
cHET
cKO
plgf-1r(Tyr1131)
/IR(Tyr1146)
Total Igf-1r
pErk1/2
(Thr202/Tyr204)
Total Erk1/2
p27
Cyclin D1
Gigyf1
GAPDH
100kDa
100kDa
55kDa
35kDa
55kDa
35kDa
27kDa
35kDa
130kDa
35kDa
Fold change in phosophorylation levels (plgf-1r/total Igf-1r)
Fold change in phosophorylation levels (pErk1/2/total Erk1/2)
Protein levels of p27
Protein levels of Cyclin D1
B
0 Days
3 Days
5 Days
7 Days
PBS
IGF-1
Gigyf1f/f
cHET
cKO
C
3 Days
5 Days
7 Days
Neurosphere diameter (μm)
Gigyf1f/f
Gigyf1f/f+IGF-1
cHET
cHET+IGF-1
cKO
cKO+IGF-1

Figure 6. Dysregulation of IGF-1R/ERK signaling in *Gigyf1* deficiency mice. (**A**) Immunoblots of pIgf-1r, Igf-1r, pErk1/2, Erk1/2, p27, cyclin D1 and Gigyf1 in lysates from brain cortical tissue of *Gigyf1*$^{f/f}$, cHET and cKO mice at E14.5. The relative levels of pIgf-1r/total Igf-1r, pErk-1r/total Erk, p27, and cyclin D1 were quantified by densitometry and compared using one-way ANOVA. (**B**) The neurosphere formation assay. Neural progenitor cells are derived from *Gigyf1*$^{f/f}$, cHET and cKO embryos. Representative images of *Gigyf1*$^{f/f}$, cHET and cKO neurosphere are shown. Scale bar represents 10 μm. (**C**) The diameters of *Gigyf1*$^{f/f}$, cHET, and cKO neurospheres were calculated and compared. Experiments were performed for three trials and the statistics is based on average of each condition from different trials. Statistic data are analyzed using one-way ANOVA and T test. All data are represented as mean ± SEM. *p<0.05, **p<0.01, ***p<0.001, ns, not significant. ****P<0.0001.